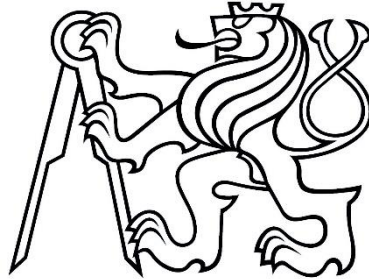


Czech Technical University in Prague
Faculty of Mechanical Engineering
Department of Instrumentation and Control Engineering



Master's Thesis

Automation of Adjustment of the Spatial Filter

Gilberto Ramos Venegas

Supervisor: doc. Ing. Jan Hošek, Ph.D.

Study Programme: Instrumentation and Control
Specialization: Optics
Master's degree

August 20, 2020



MASTER'S THESIS ASSIGNMENT

I. Personal and study details

Student's name: **Ramos Venegas Gilberto** Personal ID number: **485842**
Faculty / Institute: **Faculty of Mechanical Engineering**
Department / Institute: **Department of Instrumentation and Control Engineering**
Study program: **Mechanical Engineering**
Branch of study: **Instrumentation and Control Engineering**

II. Master's thesis details

Master's thesis title in English:

Automation of adjustment of the spatial filter

Master's thesis title in Czech:

Automatizace nastavení prostorového filtru

Guidelines:

- 1) Carry out a research for the properties and function of the spatial filter in optical systems.
- 2) Analyse necessary mechanical motions and its realisation for automation of the adjustment of the spatial filter.
- 3) Carry out the mechanical design allowing control of the spatial filter adjustment.
- 4) Propose an algorithm for automatic adjustment the of the spatial filter.

Bibliography / sources:

- [1] Trylinski, W., Fine mechanisms and precision instruments, principles of design, Pergamin Press, Warshaw, 1971,
- [2] Yoder, P., R., Jr., Opto-Mechanical system design, SpiePress, Washington, 2005
- [3] Williams D. C.: Optical Methods in Engineering Metrology, Chapman&Hall, 1993

Name and workplace of master's thesis supervisor:

doc. Ing. Jan Hošek, Ph.D., Division of precise mechanics, FME

Name and workplace of second master's thesis supervisor or consultant:

Date of master's thesis assignment: **30.03.2020** Deadline for master's thesis submission: **11.06.2020**

Assignment valid until: _____

doc. Ing. Jan Hošek, Ph.D.
Supervisor's signature

Head of department's signature

prof. Ing. Michael Valášek, DrSc.
Dean's signature

III. Assignment receipt

The student acknowledges that the master's thesis is an individual work. The student must produce his thesis without the assistance of others, with the exception of provided consultations. Within the master's thesis, the author must state the names of consultants and include a list of references.

Date of assignment receipt

Student's signature

Acknowledgements

Firstly, I would like to thank doc. Ing. Jan Hošek, Ph.D. for being my mentor during my work on this master thesis and for facilitating me access to the equipment needed for the realization of this project.

I want to thank family who, despite the distance, they have always been there for me through spirit supporting me all my life and encouraging me to pursue my personal goals.

My deepest gratitude to *Consejo Nacional de Ciencia y Tecnología* (CONACYT) for sponsoring my Master studies through the program 'Becas al Extranjero' and to the administrators and team of the regional office COECYT in Torreón, México for all their help and guidance provided.

Declaration

I declare that the present work was developed independently and that I have listed all sources of information used within it in accordance with the methodical instructions for observing the ethical principles in the preparation of university theses.

In Prague on June 20, 2020

Abstract

The objective of this thesis is to provide a Graphical user interface (GUI) for the automation of Spatial filtering. The output beam is analyzed using Image processing tools from MATLAB, the analyzed image (live video input) is processed for generating the necessary commands for output voltages which manipulate the piezo actuators which modify the position of both, the pinhole and the objective in the system with the purpose of achieving the best possible alignment and position and therefore, get a clean beam output. This GUI is intended to be easily adjusted to perform this mentioned task for many different setups.

Abstrakt

Cílem této práce je poskytnout grafické uživatelské rozhraní (GUI) pro automatizaci prostorového filtrování. Výstupní paprsek je analyzován pomocí nástrojů pro zpracování obrazu z MATLABu, analyzovaný obraz (živý video vstup) je zpracován pro generování potřebných příkazů pro výstupní napětí, která manipulují s piezoelektrickými aktory, které mění polohu obou, dírky a objektivu v systému s cílem dosáhnout nejlepšího možného vyrovnání a polohy a získat tak čistý výstup paprsku. Účelem tohoto grafického uživatelského rozhraní je snadno upravit provádění tohoto úkolu pro mnoho různých nastavení.

Key words: spatial filter, automation, piezo driver, image processing, Fourier optics.

CONTENTS

1	Introduction	1
2	Introduction to Fourier Transform.....	2
2.1.	Two-dimensional Fourier Transform	5
2.1.1	Properties of the 2-D Fourier Transform	6
2.2.	DFT and FFT.....	7
2.2.1	The Discrete Fourier Transform	8
2.2.2	The Fast Fourier Transform.....	9
3	Propagation and Diffraction	12
3.1.	Maxwell's equations.....	12
3.2.	The wave equation.....	13
3.3.	The Spatial Frequency Transfer Function for Propagation.....	14
3.4.	Diffraction	14
3.4.1	Classification of diffraction phenomena.....	17
3.4.2	Fraunhofer diffraction.....	18
4	Simulations.....	19
4.1.	Fraunhofer Diffraction through a circular aperture	19
4.2.	Fraunhofer Diffraction through a rectangular aperture.....	21
5	Goals.....	22
6	Spatial Filtering	23
7	Components and Station.....	25
7.1.	Objective and Pinhole sub-assemblies	25
7.2.	Piezo driver - P-611.XZ0	29
7.3.	Piezo driver - MIPOS 100.....	30
7.4.	T-Cube Piezo controller - TPZ001	31
7.5.	Piezo controllers' Hub.....	32
8	GUI Design	33
9	Experiment	34
9.1.	The experiment steps.....	35
9.2.	Automatic motion sequence and image capture	39
10	Results	42
11	Conclusion.....	46
	Appendix A	47
	Bibliography.....	48

LIST OF FIGURES

Figure 2.1 - Square wave function	2
Figure 2.2 - Summation of multiple sinusoidal waves	3
Figure 2.3 - Joseph Fourier's image [1]	3
Figure 2.4 - Square wave signal (a) and its fourier transfrom (b) [2], modified.....	4
Figure 2.5 - Joseph Fourier image (a) [3], real space. and its fourier transfrom (b), frequency space	5
Figure 2.6 - Computational advantage of the FFT over a direct implementation of the 1-D DFT.....	10
Figure 3.1 - Diffraction pattern of a red laser beam projected onto a plate after passing through a small circular aperture [8].	15
Figure 3.2 - Wave points' phase contribution procucing destructive interference [8].	16
Figure 3.3 - Airy disk's Minimas and Maximas diameter (y) equation [9].	16
Figure 3.4 - Regions of validity of Fresnel and Fraunhofer diffraction.	17
Figure 4.1 - Circular aperture and its diffraction pattern [7].	19
Figure 4.2 - Diffraction of red light ($\lambda=655\text{nm}$) at a circular aperture with diameter of 20 pixels. Airy disk pattern at a distance z of 49 cm.....	20
Figure 4.3 - Rectangular aperture and its diffraction pattern [7], modified.....	21
Figure 4.4 - Diffraction of blue light ($\lambda = 447\text{nm}$) at a rectangular aperture with width and height of 10 and 17 pixel unit respectively. Diffraction pattern at a distance z of 57 cm.	21
Figure 6.1 - Spatial Filter System [10].	23
Figure 6.2 - Input Gaussian Beam [10].	23
Figure 6.3 - Clean Gaussian Beam [10].	23
Figure 7.1 - Objective assembly (a) and Pinhole assambly (b) schematics.....	25
Figure 7.2 - Objective's mininum and maximum height.	26
Figure 7.3 - Designed piezo holder part 1	27
Figure 7.4 - Designed piezo holder part 2	27
Figure 7.5 - Pinhole holder.....	27
Figure 7.6 - Pinhole's mininum and maximum height.	28
Figure 7.7 - P-611.XZ0 drawing [11] modified, dimensions in mm. And Isometric 3D view with x- and y- axes legend.	29
Figure 7.8 - MIPOS 100 drawing [12], dimensions in mm. And isometric 3D view with z- axis legend..	30
Figure 7.9 - Piezo controller TPZ001 [13].	31
Figure 7.10 - TPZ001 Piezo Controller Software GUI.	31
Figure 7.11 - T-Cube USB Controller Hub (left), Power Supply Unit (right) [14].	32
Figure 8.1 - Graphical User Interface for the control and image capture of diffraction patterns.	33
Figure 9.1 - GUI app, piezo driver motion and image capture experimental setup.....	34
Figure 9.2 - Initiated Spatial Filter application.	35
Figure 9.3 - TPZ001 controllers connection initiated.....	36
Figure 9.4 - Folder selection for saving images.	36
Figure 9.5 - MATLAB's Image Acquisition Tool. Selected camera format and region of interest.	37
Figure 9.6 - ROIPosition	38
Figure 9.7 - GUI, camera format and ROI position defined.....	38

Figure 9.8 - Diffraction pattern shown in the user interface at 57.66V (x-axis), 25V (y-axis) and 60V (z-axis) supply.....	39
Figure 9.9 - Pinhole's displacement ($1V \approx 1\mu m$).....	39
Figure 9.10 - Area of best Airy disk detection (left), becomes next analysis area for the second iteration (right).....	40
Figure 10.1 - Diffraction patterns (left), and their 2D Fourier Transform (right).	42
Figure 10.2 - Region of analysed images.	44
Figure 10.3 - Proposed Symmetry analysis for next development.	45

LIST OF TABLES

Table 2.1 - Properties of the Fourier transform (a, b, kx_0 and ky_0 are real nonzero constants; m and n are non-negative integers).	7
Table 7.1 - Sub-assemblies a and b components.....	26
Table 7.2 - Hub Supply coltage and current requirements.	32

ABBREVIATIONS AND TERMS

DFT	Discrete Fourier Transform
FFT	Fast Fourier Transform
FT	Fourier Transform
GUI	Graphical User Interface
ODE	Ordinary Differential Equation
PDE	Partial Differential Equation
SF	Spatial Filter
ROI	Region of Interest

1 Introduction

The ultimate task of a Spatial filter is to process a coherent input beam of light (laser source) and deliver a *cleaned-up* output beam. Sometimes a laser system does not produce a beam with a smooth intensity profile, so in order to produce a clean Gaussian beam, a spatial filter is used to remove the unwanted multiple-order energy peaks and pass only the central maximum of the diffraction pattern. When a laser beam passes through a system, dust in the air or on optical components can disrupt the beam and create scattered light. This scattered light can leave unwanted ring patterns in the beam profile. The spatial filter removes also these additional spatial noises from the system.

The spatial filter assembly consists of a focal lens/microscope objective, a pinhole aperture, and a positioning mechanism. The positioning mechanism has precision X-Y movements which center the pinhole at the focal point of the objective lens.

Spatial filter systems are important for many applications where interferometry is applied, particularly in holography, where spatial intensity variations in the laser beam are undesirable, hence the creation of a uniform gaussian beam for such application is very crucial.

The main task for this thesis project is to design an application capable to manipulate the pinhole's location to a precise position where the produced output beam would reflect that of a clean Gaussian Beam.

2 Introduction to Fourier Transform

This chapter will be mainly an introduction to the Fourier Transform (FT) and its mathematical equations used in optics. The FT, transforms a function in the time domain $f(t)$ or in the spatial domain $f(x)$, into the frequency domain $f(\omega)$ and $f(k)$ where $\omega=2\pi f$ and $k=2\pi f_s$. The spatial frequency f_s is defined as the number of wavelengths in a unit of distance: $f_s = 1/\lambda$ [1/mm]. The FT also transforms its inverse as well.

$$F(k) = \int_{-\infty}^{\infty} f(x)e^{-j2\pi kx} dx \quad (2.1.1)$$

$$f(x) = \int_{-\infty}^{\infty} F(k)e^{j2\pi kx} dk \quad (2.1.2)$$

The Eq. (2.0.1) shows the Fourier transform of a function in the spatial domain (one-dimensional) and its inverse is shown in Eq. (2.0.2).

The harmonics (sines and cosines) in these equations are then introduced by the Euler's formula:

$$e^{jx} = \cos x + j\sin x \quad (2.1.3)$$

$$e^{-jx} = \cos x - j\sin x \quad (2.1.4)$$

As an example of the utility of the FT, let us assume a square wave function (spatial domain) as shown in Figure 2.1.

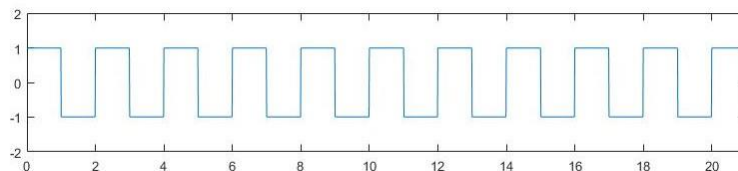


Figure 2.1 - Square wave function

This square wave can then be approximated as a summation of multiple sine waves of different amplitudes and frequencies as shown below:

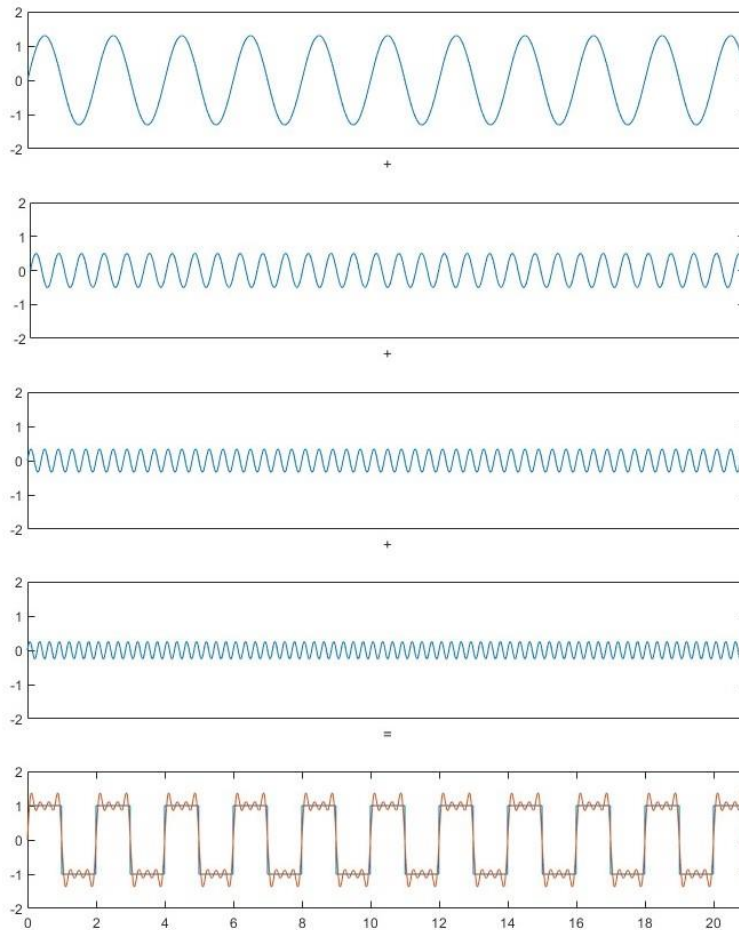


Figure 2.2 - Summation of multiple sinusoidal waves

As seen above in Figure 2.2, when multiple sinusoidal waves of different amplitudes and frequencies are super-imposed their interference generates another resulting periodic function, a square wave signal in our example, for which the more sinusoidal waves are added to this summation then the approximation to the square signal gets closer.

Any function can then be represented in terms of spatial frequencies. And this is important because any waveform or image can be expressed as the superposition of numerous harmonics. The more harmonics you are willing to have, the closer representation of the original waveform or image.

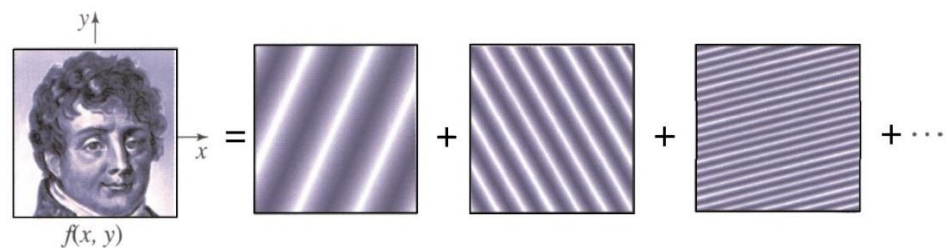


Figure 2.3 - Joseph Fourier's image [1]

As shown by Heikenfeld in Figure 2.3 [1]; it exhibits an example of how an image, spatial function $f(x, y)$, can be represented with a summation on these harmonic waves. Now to have a real perception of what the Fourier transform of an image looks like let's consider the single square wave signal from figure 2.1 this time as being 'seen from above' as presented by Huang in Figure 2.4(a) [2] and also lets consider Eq. (2.0.1) and (2.0.3) which in this case as the square signal propagates in the x-axis we get the following FT represented as a summation to get:

$$f(x) = \sum F(k) \sin(xk_x) \quad (2.1.5)$$

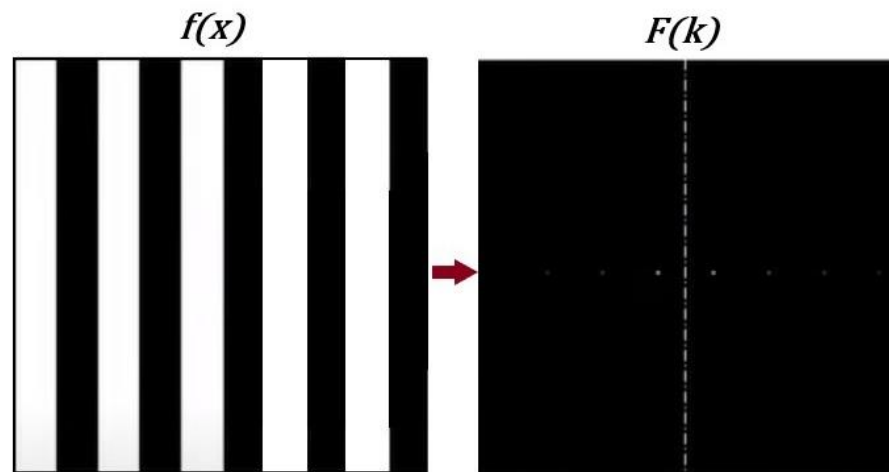


Figure 2.4 - Square wave signal (a) and its fourier transform (b) [2], modified

The position of each dot in the Fourier transform $F(k)$ as shown above in Figure 2.4(b) [1] describe the spatial frequency, and the intensity of the dots is what describes the amplitude. The further away the dot is located from the center the higher the frequency of the harmonic while the closer to the center point represents the lower frequencies. The intensity of these spots essentially describes the amplitude of the harmonics, with the higher amplitudes being showed as brighter dots, and dimmer dots for the lower amplitudes.

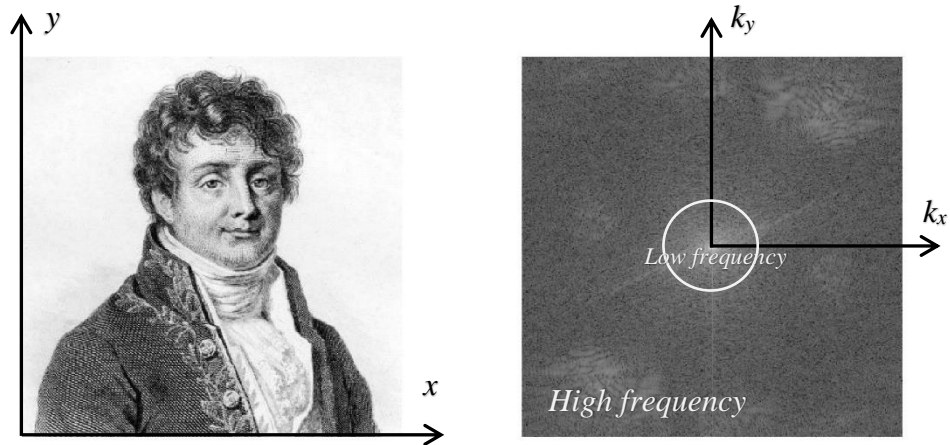


Figure 2.5 - Joseph Fourier image (a) [3], real space. and its fourier transform (b), frequency space

As reference from Figure 2.4 [2]; and portrait retrieved from the Wikipedia biography [3] of the mathematician and physicist Jean-Baptiste Joseph Fourier it was produced this image's Fourier transform which can be observed above in Figure 2.5(b), where the low frequencies are clearly shown at the centermost while the higher frequencies which make up this image are located outside of this center region.

2.1. Two-dimensional Fourier Transform

The 2-D Fourier transform equation of a spatial domain signal $f(x, y)$, $-\infty < x, y < \infty$ is defined by:

$$F(k_x, k_y) = \sum_{x=-\infty}^{\infty} \sum_{y=-\infty}^{\infty} f(x, y) e^{-j2\pi(xk_x + yk_y)} \quad (2.1.1)$$

Or by its integral solution as:

$$\begin{aligned} F(k_x, k_y) &= \int_{-\infty}^{\infty} \int_{-\infty}^{\infty} f(x, y) e^{-j2\pi(xk_x + yk_y)} dx dy \quad (2.1.2) \\ &= F_{xy}\{f(x, y)\} \end{aligned}$$

where k_x and k_y are the spatial frequencies corresponding to the x- and y-directions, respectively.

Its inverse transform is given by:

$$f(x, y) = \int_{-\infty}^{\infty} \int_{-\infty}^{\infty} F(k_x, k_y) e^{j2\pi(ux+vy)} dk_x dk_y \quad (2.1.3)$$

$$= F_{xy}^{-1}\{F(k_x, k_y)\}$$

2.1.1 Properties of the 2-D Fourier Transform

The properties of the 2-D Fourier transform are generalizations of the 1-D Fourier transform. We will need the definitions of even and odd signals in 2-D.

A signal $f(x, y)$ is *even (symmetric)* if:

$$f(x, y) = f(-x, -y) \quad (2.1.4)$$

$f(x, y)$ is *odd (antisymmetric)* if:

$$f(x, y) = -f(-x, -y) \quad (2.1.5)$$

These definitions indicate two-fold symmetry and it is possible to extend them to four-fold symmetry in 2-D.

The main properties of the Two-dimension Fourier Transform are summarized in table 2-1 below.

Table 2.1 - Properties of the Fourier transform (a, b, kx_0 and ky_0 are real nonzero constants; m and n are non-negative integers).

Property	$f(x, y)$	$F(k_x, k_y)$
1. Linearity	$au_1(x, y) + bu_2(x, y)$	$aU_1(k_x, k_y) + bU_2(k_x, k_y)$
2. Convolution	$u_1(x, y) * u_2(x, y)$	$U_1(k_x, k_y)U_2(k_x, k_y)$
3. Correlation	$u_1(x, y) \circ u_2(x, y)$	$U_1(k_x, k_y)U_2^*(k_x, k_y)$
4. Modulation	$u_1(x, y)u_2(x, y)$	$U_1(k_x, k_y) * U_2(k_x, k_y)$
5. Separable function	$u_1(x)u_2(y)$	$U_1(k_x)U_2(k_y)$
6. Space shift	$u(x - x_0, y - y_0)$	$e^{-j2\pi(k_x x_0 + k_y y_0)} \bullet U(k_x, k_y)$
7. Frequency shift	$e^{j2\pi(k_{x0}x + k_{y0}y)} \bullet u(x, y)$	$U(k_x - k_{x0}, k_y - k_{y0})$
8. Differentiation in space domain	$\frac{\partial^m}{\partial x^m} \frac{\partial^n}{\partial y^n} u(x, y)$	$(j2\pi k_x)^m (j2\pi k_y)^n U(k_x, k_y)$
9. Differentiation in Frequency domain	$(-j2\pi x)^m (-j2\pi y)^n u(x, y)$	$\frac{\partial^m}{\partial k_x^m} \frac{\partial^n}{\partial k_y^n} U(k_x, k_y)$
10. Laplacian in the state space	$\left(\frac{\partial^2}{\partial x^2} + \frac{\partial^2}{\partial y^2}\right)u(x, y)$	$-4\pi^2(k_x^2 + k_y^2)U(k_x, k_y)$
11. Laplacian in the frequency domain	$-4\pi^2(x^2 + y^2)u(x, y)$	$\left(\frac{\partial^2}{\partial k_x^2} + \frac{\partial^2}{\partial k_y^2}\right)U(k_x, k_y)$
12. Square of signal	$ u(x, y) ^2$	$U(k_x, k_y) * U^*(k_x, k_y)$
13. Square of spectrum	$u(x, y) * u^*(x, y)$	$ U(k_x, k_y) ^2$
14. Rotation of axes	$u(\pm x, \pm y)$	$U(\pm k_x, \pm k_y)$
15. Parseval's theorem	$\int_{-\infty}^{\infty} \int_{-\infty}^{\infty} u(x, y)g^*(x, y)dx dy = \int_{-\infty}^{\infty} \int_{-\infty}^{\infty} U(k_x, k_y)G^*(k_x, k_y)dk_x dk_y$	
16. Real $u(x, y)$	$U(k_x, k_y) = U^*(-k_x, -k_y)$	
17. Real and even $u(x, y)$	$U(k_x, k_y)$ is real and even	
18. Real and odd $u(x, y)$	$U(k_x, k_y)$ is imaginary and odd	

2.2. DFT and FFT

Although a brief introduction to the Fourier Transform has been made, it is now essential to have a clear understanding of how the FT itself can be used for image processing. This is now why the Discrete Fourier Transform and the Fast Fourier Transform are now explained in a manner which may clarify their fundamentals and explain their relevance to digital image processing.

2.2.1 The Discrete Fourier Transform

The discrete Fourier transform (DFT) of a periodic sequence $f(x)$ of length M is defined as:

$$F(k) = \frac{1}{\sqrt{M}} \sum_{x=0}^{M-1} f(x) e^{-j2\pi xk/M} \quad (2.2.1)$$

with the inverse 1-D DFT given by:

$$f(x) = \frac{1}{\sqrt{M}} \sum_{k=0}^{M-1} F(k) e^{j2\pi xk/M} \quad (2.2.2)$$

The DFT defined above is orthonormal. The equation can then be further simplified if normality is not required as follow:

$$F(k) = \frac{1}{M} \sum_{x=0}^{M-1} f(x) e^{-j2\pi xk/M} \quad (2.2.3)$$

$$f(x) = \sum_{k=0}^{M-1} F(k) e^{j2\pi xk/M} \quad (2.2.4)$$

Note that the constant $1/M$ was placed in front of the DFT, but it can be placed in front of either one, the DFT or its inverse equation.

Now, the two-dimensional DFT is like a decomposition of an image into complex exponentials (sines & cosines). Which is a very powerful method to use for Image processing systems, therefore we must get familiarized with its principle and its formulas. The 2-D DFT is obtained from the 1-D DFT by applying the one-dimensional discrete Fourier transform first to the rows of a signal matrix, and then to its columns or vice versa. For a 2-D periodic sequence given by $f(x, y)$, $0 \leq x < M$, $0 \leq y < N$, its 2-D DFT can be written as:

$$F(k_x, k_y) = \frac{1}{MN} \sum_{x=0}^{M-1} \sum_{y=0}^{N-1} f(x, y) e^{-j2\pi(\frac{xk_x}{M} + \frac{yk_y}{N})} \quad (2.2.5)$$

with the inverse 2-D DFT given by:

$$f(x, y) = \sum_{k_x=0}^{M-1} \sum_{k_y=0}^{N-1} F(k_x, k_y) e^{j2\pi(\frac{xk_x}{M} + \frac{yk_y}{N})} \quad (2.2.6)$$

their formulas by integration are as follow:

$$F(k_x, k_y) = \frac{1}{MN} \int_{x=0}^{M-1} \int_{y=0}^{N-1} f(x, y) e^{-j2\pi(\frac{xk_x}{M} + \frac{yk_y}{N})} dx dy \quad (2.2.7)$$

$$f(x, y) = \int_{k_x=0}^{M-1} \int_{k_y=0}^{N-1} F(k_x, k_y) e^{j2\pi(\frac{xk_x}{M} + \frac{yk_y}{N})} dk_x dk_y \quad (2.2.8)$$

For our case in Image processing our discrete Fourier transform function $f(x, y)$ will represent the images of size $M \times N$ which will be analyzed with the given equations above.

2.2.2 The Fast Fourier Transform

As mentioned by Poon *et al.* [4] and Gonzalez and Woods [5] The DFT is a way of numerically approximate the continues Fourier transform of a function, and the main reason the DFT is of great interest in signal processing is due its efficient and rapid evaluatin by using the developed fast Fourier transform. For instance, the computation of the one-dimensional DFT (2.2.3) of M points directly requires M^2 multiplication/addition operations, thus for the case where $M = 1024$, the method would require 10^6 operations; meanwhile the FFT accomplishes the same task on the order of $M \cdot \log_2 M$ operations resulting in about 10^4 operations for the same value of M , which in this case ($M = 1024$) the computational advantage is of 100 to 1. Something to consider is that for bigger problems this computational advantage also increases. If, for instance, $M = 16384(2^{14})$, the computational advantage grows to 1170 to 1. This is a great reason of why working with FFT is fundamental.

The computational advantage of the FFT over a direct implementation of the 1-D DFT is defined as

$$\begin{aligned}
C(M) &= \frac{M^2}{M \cdot \log_2 M} \\
&= \frac{M}{\log_2 M}
\end{aligned}
\tag{2.2.9}$$

And because it is assumed that $M = 2^n$, we can express Eq. (2.2.9) in terms of n :

$$C(n) = \frac{2^n}{n}
\tag{2.2.10}$$

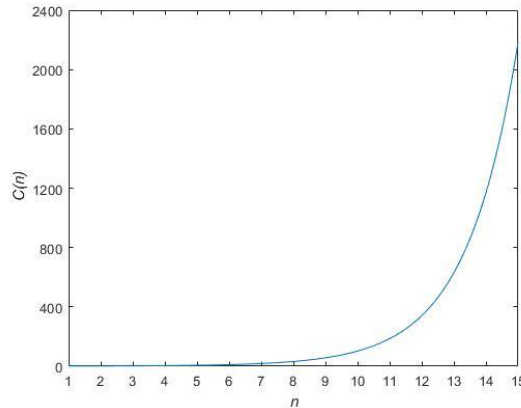


Figure 2.6 - Computational advantage of the FFT over a direct implementation of the 1-D DFT

The software MATLAB has the built-in function: $Y = fft(X)$; which computes the discrete Fourier transform of X using a fast Fourier transform algorithm [6]:

- If X is a vector, then $fft(X)$ returns the Fourier transform of the vector.
- If X is a matrix, then $fft(X)$ treats the columns of X as vectors and returns the Fourier transform of each column.

We can then obtain the inverse FFT in MATLAB with the function: $X = ifft(Y)$, Nevertheless, the FFT function in MATLAB returns the Fourier transform of each column for the case that X is a matrix (image), when in fact we need a two-dimensional Fourier transform. This 2-D FT is simply achieved by using the function $Y = fft2(X)$; for which the inverse is defined as: $X = ifft2(Y)$.

These FFT functions are very important for this project as they ease the image processing methods to be implemented to achieve the goal. And though MATLAB's functions are very convenient tools it is also very important to understand what is behind this FFT algorithm, hence it shall be explained. Let's express Eq. (2.2.3) for notational convenience as:

$$F(u) = \frac{1}{N} \sum_{x=0}^{N-1} f(x) W_N^{ux} \quad (2.2.11)$$

where

$$W_N = e^{-j2\pi/N} \quad (2.2.12)$$

and N is assumed to be of the form and n being a positive integer. Therefore, N can be expressed as

$$N = 2^n = 2K \quad (2.2.13)$$

With K also being a positive integer. Substitution Eq. (2.2.12) into Eq. (2.2.9) gives:

$$\begin{aligned} F(u) &= \frac{1}{2K} \sum_{x=0}^{2K-1} f(x) W_{2K}^{ux} \\ &= \frac{1}{2} \left[\frac{1}{K} \sum_{x=0}^{K-1} f(2x) W_{2K}^{u(2x)} + \frac{1}{K} \sum_{x=0}^{K-1} f(2x+1) W_{2K}^{u(2x+1)} \right] \end{aligned} \quad (2.2.14)$$

Furthermore, after few more mathematical steps we obtain the equation:

$$F(u+K) = \frac{1}{2} [F_{even}(u) - F_{odd}(u) W_{2K}^u] \quad (2.2.15)$$

where:

$$F_{even}(u) = \frac{1}{K} \sum_{x=0}^{K-1} f(2x) W_K^{ux} \quad (2.2.16)$$

$$F_{odd}(u) = \frac{1}{K} \sum_{x=0}^{K-1} f(2x+1) W_K^{ux} \quad (2.2.17)$$

both for $u = 0, 1, 2, \dots, K-1$.

3 Propagation and Diffraction

Wave optics accounts for the effect of diffraction which is important to know prior proceeding to the experimental process and analysis of the project. Therefore, in this chapter it is introduced the wave optics through Maxwell's equations. We then review diffraction using Fourier transforms as well as the Spatial transfer function and the impulse response of propagation. To later continue to the next chapter where this set of equations will be used to create diffraction simulations of plane waves passing through circular and rectangular/square aperture shapes.

3.1. Maxwell's equations

The mathematical model which unites electricity, magnetism, and light into one phenomenon was formulated by Scottish scientist James Clerk Maxwell (1831-1879). In electromagnetics, we are concerned with four vector quantities called electromagnetic fields: the electric flux density (electric induction) \vec{D} [C/m²], the magnetic flux density (magnetic induction) \vec{B} [Wb/m²], the electric field strength (electric vector) \vec{E} [V/m], and the magnetic field strength (magnetic vector) \vec{H} [A/m]. These set of four equations are known as the Maxwell's equations and are expressed in their differential form as:

$$\text{div}\vec{D} = \rho \quad (3.1.1)$$

$$\text{div}\vec{B} = 0 \quad (3.1.2)$$

$$\text{rot}\vec{E} = -\frac{\partial\vec{B}}{\partial t} \quad (3.1.3)$$

$$\text{rot}\vec{H} = \vec{J} = \vec{J}_c + \frac{\partial\vec{D}}{\partial t} \quad (3.1.4)$$

Where t is time [s], \vec{J} is the electric current density [A/m²] and ρ is the electric charge density [C/m³]. \vec{J}_c and ρ are the sources which generate the electromagnetic fields.

The equation (3.1.1) is the differential representation of the Gauss's law for electric fields and can be converted to its integral form by integration over a volume V bounded to a surface S and using the *divergence theorem*. The integral form of equation (3.1.2), the *magnetic analog* of Eq. (3.1.1), can be obtained similarly by using the divergence theorem. *Faraday's law of induction* defined by Eq. (3.1.3) and the *Generalized Ampere Law*, Eq.

(3.1.4), are converted to their integral forms by integration over an open surface S bounded by a line C and using the *Stroke's theorem*. The integral forms are then defined by the following equations:

$$\oint_S \vec{D} \cdot d\vec{S} = \int_V \rho dV \quad (3.1.5)$$

$$\oint_S \vec{B} \cdot d\vec{S} = 0 \quad (3.1.6)$$

$$\oint_C \vec{E} \cdot d\vec{l} = - \int_S \frac{\partial \vec{B}}{\partial t} \cdot d\vec{S} \quad (3.1.7)$$

$$\oint_C \vec{H} \cdot d\vec{l} = \int_S \frac{\partial \vec{D}}{\partial t} \cdot d\vec{S} + \int_S \vec{J}_c \cdot d\vec{S} \quad (3.1.8)$$

3.2. The wave equation

By manipulations with Maxwell's equations we can obtain differential equations for which each field vector must separately satisfy. Conditions are: homogeneous isotropic dielectric, permittivity and permeability constant in time.

Used formulas:

$$\vec{A} \times \vec{B} \times \vec{C} = (\vec{A} \cdot \vec{C}) \vec{B} - (\vec{A} \cdot \vec{B}) \vec{C} \quad \text{rot} \vec{A} = \nabla \times \vec{A} \quad \text{div} \vec{A} = \nabla \cdot \vec{A}$$

Wave equation:

$$\nabla^2 \vec{E} = \varepsilon \mu \frac{\partial^2 \vec{E}}{\partial t^2} \quad (3.2.1)$$

Scalar wave equation from acoustic:

$$\nabla^2 u(x, y, z, t) = \frac{1}{v^2} \frac{\partial^2 u(x, y, z, t)}{\partial t^2} \quad (3.2.2)$$

The instantaneous amplitude of a particle is: u

The exciment propagation velocity in the medium: v

The term $\frac{1}{\sqrt{\varepsilon \mu}}$ has unit of velocity. Maxwell concluded that Eq. (3.2.1) is an *equation of an electromagnetic vector wave motion*.

The velocity for this waves is $v = \frac{1}{\sqrt{\varepsilon \mu}}$ and $c = \frac{1}{\sqrt{\varepsilon_0 \mu_0}} = 299\,798\,458 \text{ m/s}$ in vacuum, which represents the speed of light (c).

3.3. The Spatial Frequency Transfer Function for Propagation

According to Poon et. al. [4] and [7]; in Fourier optics, the known *Free-space spatial impulse response function*, $h(x, y; z)$, is defined as:

$$h(x, y; z) = h_0 \cdot \exp \left[-jk_0 \frac{(x^2 + y^2)}{2z} \right] \quad (3.3.1)$$

where:

$$h_0 = \left(\frac{jk_0}{2\pi z} \right) \cdot \exp(-jk_0 z) \quad (3.3.2)$$

$$k_0 = \frac{2\pi}{\lambda} \quad (3.3.3)$$

therefore, the Free-space impulse response function can be expressed as:

$$h(x, y; z) = \left(\frac{j}{\lambda z} \right) \cdot \exp \left(\frac{-j2\pi z}{\lambda} \right) \cdot \exp \left(\frac{-j\pi(x^2 + y^2)}{\lambda z} \right) \quad (3.3.4)$$

Now, by taking the 2-D Fourier transform of Eq. (3.3.1), we obtain:

$$\begin{aligned} H(k_x, k_y; z) &= F_{xy}\{h(x, y; z)\} \\ &= \exp(-jk_0 z) \cdot \exp \left[\frac{j(k_x^2 + k_y^2)z}{2k_0} \right] \end{aligned} \quad (3.3.5)$$

$H(k_x, k_y; z)$ is called the *spatial frequency response* in Fourier Optics.

3.4. Diffraction

Light waves, circular or planar, when passing through an aperture gets *diffracted*. And according to its definition, the *bending* of a wave or its *deviation* from the original direction of propagation when it meets a small obstacle is called *Diffraction*. This phenomenon is important to understand as the purpose of this thesis work is to analyze the diffraction pattern of the laser beam source passing through a pinhole (the aperture/obstacle), with the purpose to obtain a clean output beam.

Diffraction occurs with all types of waves, such as electromagnetic waves (light), acoustical waves, ultrasonic waves and radio waves among others.

The behavior of wave fields passing through obstacles cannot be simply described in terms of rays. For example, when a plane wave passes through an aperture, some of the wave deviates from its original direction of propagation, and the resulting wave field is different from the wave field passing initially through the aperture, both in size and shape [7].

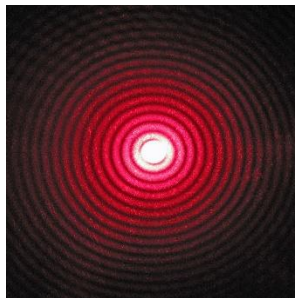


Figure 3.1 - Diffraction pattern of a red laser beam projected onto a plate after passing through a small circular aperture [8].

The projected diffraction interference pattern shown above in Figure3.1 is a result of a source beam (red laser → planar wavefront) passing through a small circular aperture located in front of a plane different to the projection plane. A simple explanation of why this occurs, we need to understand that each wave can be thought of as the combination of an infinite number of smaller waves which spread out in all directions. When the wave hits an obstacle or a hole/aperture, only the portion of the wave that is directly behind the hole is able to pass through. In Figure3.2, it is shown how these infinite number of smaller wave points (3 shown) interfere at a point $-\theta_{MIN,0}$ in the first minima of the diffraction pattern.

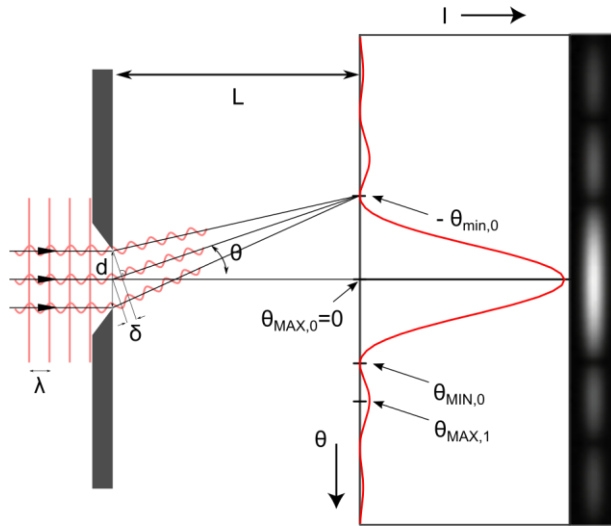


Figure 3.2 - Wave points' phase contribution producing destructive interference [8].

Light and waves in general can interfere both, constructively and destructively.

Constructive interference occurs when the resultant wave amplitude at a given point has a greater amplitude than the individual waves forming the interference; on the other hand, destructive interference is the resultant wave which has a lower amplitude than the individual waves which are interference. For complete destructive interference waves which interfere must have a phase difference of π ($\frac{\lambda}{2}$).

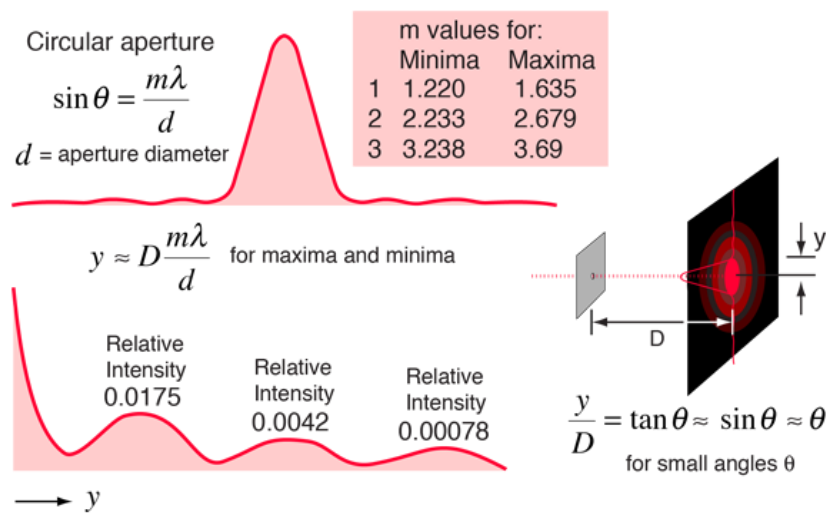


Figure 3.3 - Airy disk's Minimas and Maximas diameter (y) equation [9].

For the case of Circular apertures the Airy disk's Minimas and Maximas diameter ($2*y$) can be calculated as shown in Figure 3.3.

From this figure, it can be said that far from the aperture, the angle at which the first minima occurs is given by the formula:

$$\sin\theta = 1.22 \frac{\lambda}{d} \quad (3.4.1)$$

and for very small angles, considering $\frac{y}{D} = \tan\theta \approx \sin\theta \approx \theta$, the formula is simply:

$$\theta \approx 1.22 \frac{\lambda}{d} \quad (3.4.2)$$

Please note that for Eq. (3.4.1) θ is in degrees and in Eq. (3.4.2) is in radians. Distance D and aperture diameter d as well as light's wavelength λ can all have same unit in meters.

3.4.1 Classification of diffraction phenomena

The region of validity of Fraunhofer diffraction are shown in Figure 3.4.

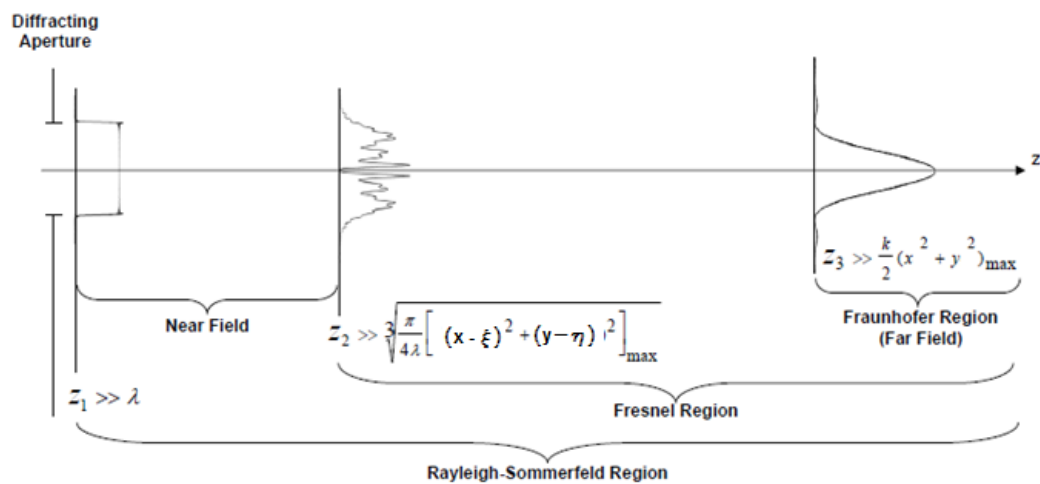


Figure 3.4 - Regions of validity of Fresnel and Fraunhofer diffraction.

3.4.2 Fraunhofer diffraction

The Fraunhofer diffraction pattern at the plane point $P(x, y)$ is proportionat to the squared magnitude of the Fourier transform of the aperture function $P_0(x', y')$ evaluated at the spatial frequencies $v_x = x/\lambda d$ and $v_y = y/\lambda d$.

Second order tems are neglected and some additional simplification to the Fraunhofer diffraction is made by introducing reduced coordinates u and v of the point of observation P relative to the source point P_0 .

$$u = \frac{l - l_0}{\lambda} = \frac{a}{\lambda} \quad (3.4.3)$$

$$v = \frac{m - m_0}{\lambda} = \frac{b}{\lambda} \quad (3.4.4)$$

their units [1/m], as the unit of space frequency.

The constant placed before the diffraction integral is given by:

$$C = -\frac{jk}{2\pi} \cos\delta \cdot a \frac{e^{jk(R+R_0)}}{R \cdot R_0} \quad (3.4.5)$$

The amplitude transmissivity of the screen or the *aperture funtion* (a ratio of complex amplitudes just before and just behind the screen):

$$p_0(x, y) = \frac{u(x, y)}{u_0(x, y)} = \begin{cases} 0, & \text{outside the aperture} \\ 1, & \text{inside the aperture} \end{cases} \quad (3.4.6)$$

From this, then the Fraunhofer integral equation of diffraction becomes:

$$P(x, y) = C \int_{-\infty}^{\infty} \int_{-\infty}^{\infty} p_0(x, y) \cdot e^{-j2\pi(ux+vy)} dx dy \quad (3.4.7)$$

4 Simulations

In this chapter it is explained some concepts of the simulations carried out during the process for solution of this thesis' main task. The applications developed which are mentioned are publicly available at <https://github.com/gilramosx/SpatialFilter>.

4.1. Fraunhofer Diffraction through a circular aperture

The analysis of diffraction through circular apertures is one of major importance in the study of Fourier Optics since this is the shape of most optical devices for image capture or visualization, i.e. cameras, telescopes, microscopes and also the final receptor of every image, the human eye (round-shaped pupil).

Therefore, the application file *FraunhoferDiffraction.mlapp*, GUI shown in Figure 4.1 and Figure 4.2, can be found in the attachments of Appendix A; in this application the user can simulate the diffraction pattern of light passing through a circular aperture where parameters such as distance z (diffraction pattern plane from aperture plane), light wavelength λ , and circular aperture's radius (unit in pixels) can all be modified showing the change in the simulated diffraction pattern.

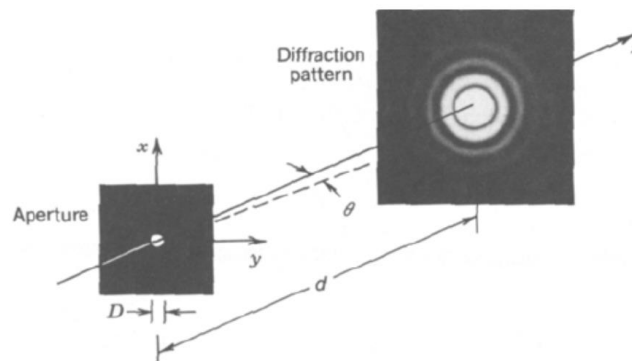


Figure 4.1 - Circular aperture and its diffraction pattern [7].

The intensity of the diffraction pattern of a circular aperture (Airy disk), at a certain point in the observation plane is given by the equation:

$$I(x, y) = I_0 \left[\frac{2J_1(\pi D \rho / \lambda d)}{\pi D \rho / \lambda d} \right]^2 \quad (4.1.1)$$

where:

$$\rho = (x^2 + y^2)^{1/2} \quad (4.1.2)$$

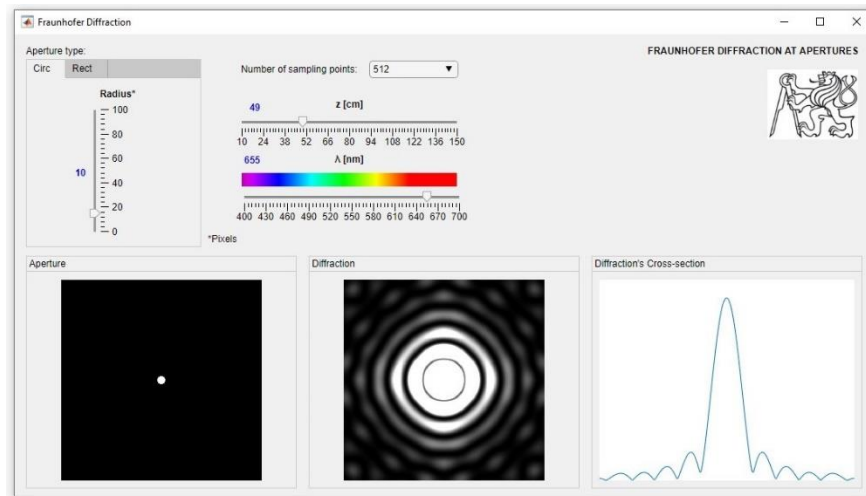


Figure 4.2 - Diffraction of red light ($\lambda=655\text{nm}$) at a circular aperture with diameter of 20 pixels. Airy disk pattern at a distance z of 49 cm.

4.2. Fraunhofer Diffraction through a rectangular aperture

Similarly, as in the diffraction through a circular aperture, the application *FraunhoferDiffraction.mlapp* also has the function to simulate square aperture shapes.

The *aperture function* [as Eq. (3.4.6)] for rectangular apertures where the height and the width are represented by a and b respectively, is given by:

$$p_0(x, y) = \Pi\left(\frac{x}{a}\right) \Pi\left(\frac{y}{b}\right)$$

$$p_0(x, y) = \text{rect}\left(\frac{x}{a}\right) \text{rect}\left(\frac{y}{b}\right) \quad (4.2.1)$$

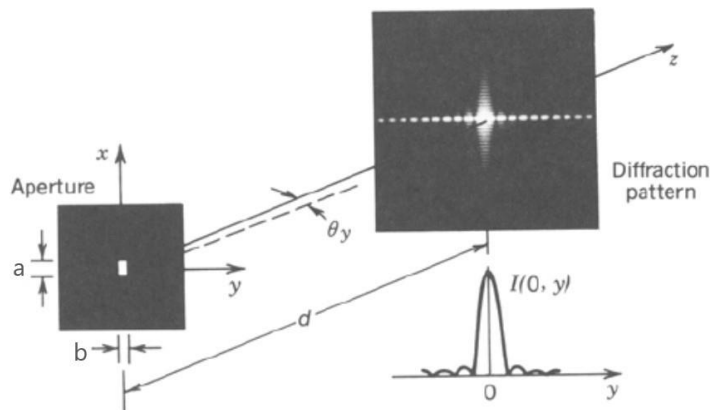


Figure 4.3 - Rectangular aperture and its diffraction pattern [7], modified.

The intensity is proportional to the squared absolute value of the Fraunhofer diffraction equation, Eq. (3.4.7).

$$|P(x, y)|^2 \rightarrow I(x, y) = I_0 \cdot \text{sinc}^2\left(\frac{ax}{\lambda d}\right) \cdot \text{sinc}^2\left(\frac{by}{\lambda d}\right) \quad (4.2.2)$$

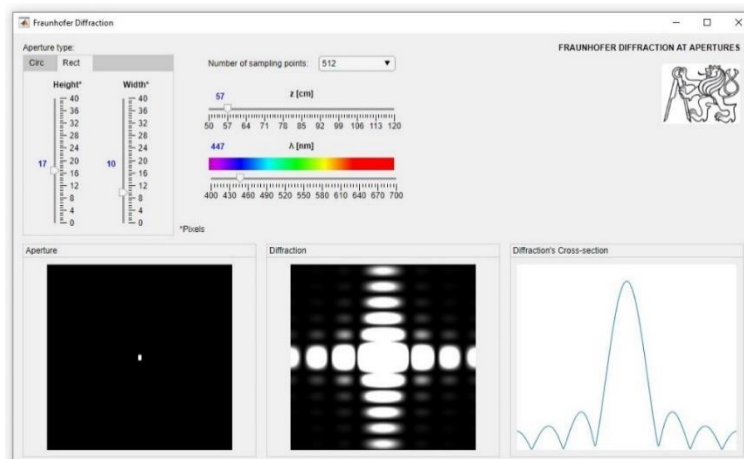


Figure 4.4 - Diffraction of blue light ($\lambda = 447\text{nm}$) at a rectangular aperture with width and height of 10 and 17 pixel unit respectively. Diffraction pattern at a distance z of 57 cm.

5 Goals

Based on the thesis' guidelines, several goals have been set. The following tasks have been laid out.

1. Carry out a research for the properties and function of the spatial filter in optical systems.
2. Analyze necessary mechanical motions and its realization for automation of the adjustment of the spatial filter.
3. Carry out the mechanical design allowing control of the spatial filter adjustment.
4. Propose an algorithm for the automatic adjustment of the spatial filter.

6 Spatial Filtering

For many applications, such as holography, spatial intensity variations in the laser beam are unacceptable. Therefore, a spatial filter system is ideal for producing a clean Gaussian beam.

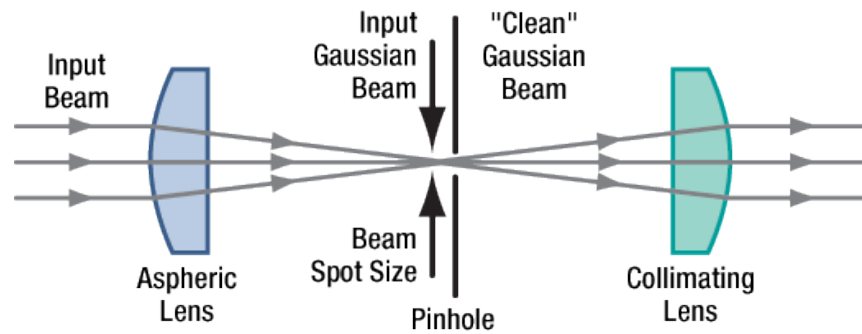


Figure 6.1 - Spatial Filter System [10].

The input Gaussian beam has spatially varying intensity "noise". When a beam is focused by an aspheric lens, the input beam is transformed into a central Gaussian spot (on the optical axis) and side fringes, which represent the unwanted "noise" (see Figure 6.2). The radial position of the side fringes is proportional to the spatial frequency of the "noise".

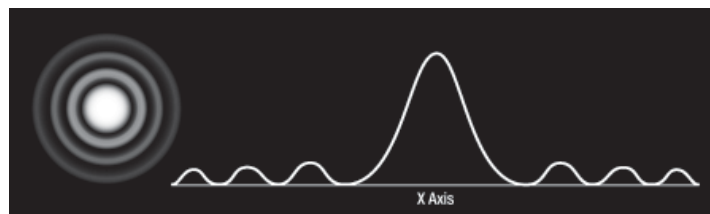


Figure 6.2 - Input Gaussian Beam [10].

By centering a pinhole on a central Gaussian spot, the "clean" portion of the beam can pass while the "noise" fringes are blocked (see Figure 6.3).

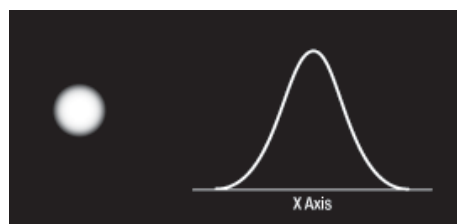


Figure 6.3 - Clean Gaussian Beam [10].

The diffraction-limited spot size at the 99% contour is given by:

$$D = \frac{\lambda f}{r} \quad (4.2.1)$$

where:

λ = Wavelength [μm]

f = Lens focal length [mm]

r = Input beam radius [mm] at $I_0 \cdot e^{-2}$

7 Components and Station

Certain requirements should be met when carrying out this experiment; besides a vibration isolating table/board, every other component must be rigid and fixed accordingly. The whole system has been divided into two main subassemblies for its description and function as follow:

7.1. Objective and Pinhole sub-assemblies

The purpose of the objective's assembly is to house the objective and its piezo actuator in a magnetically-fixed seat which holds a single-axis (horizontal) linear stage for manual setting approximation, see Figure 7-1.

Meanwhile, the pinhole's assembly has the same purpose for the target component (pinhole). This assembly consists of a main base with 3-axis stage with a travel range of 25 mm in each direction (resolution 10 μm), the pinhole itself and its 2-axis piezo drive.

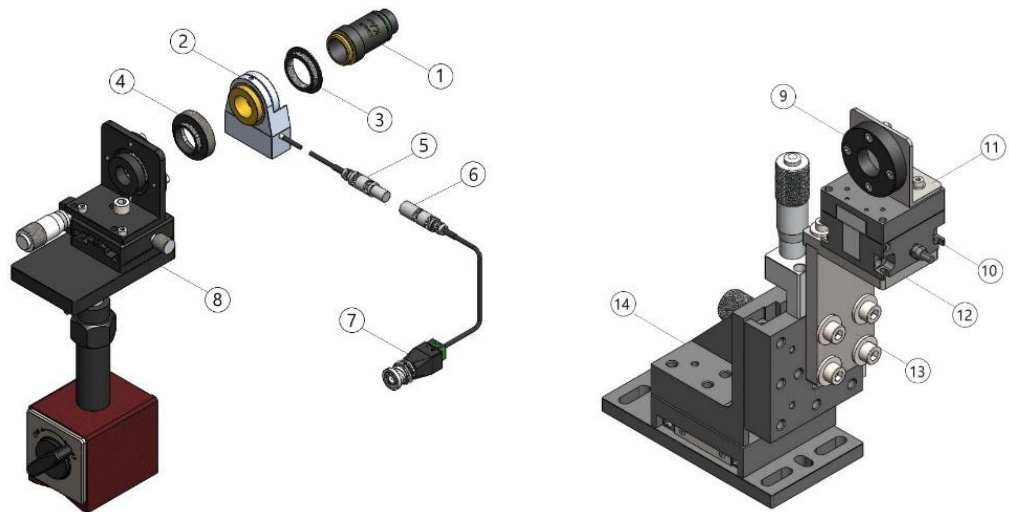


Figure 7.1 - Objective assembly (a) and Pinhole assembly (b) schematics.

The components of these assemblies are listed next in Table 7.1:

Table 7.1 - Sub-assemblies a and b components

	Component	Brand	Model/Characteristics
1	Objective	Melles Griot	
2.	Piezo drive	Piezosystem Jena	MIPOS 100
3.	Adapter		RMS to M25
4.	Adapter		M25 to RMS
5.	Connector	Lemo	FFA.0S.302.CLAC37
6.	Connector	Lemo	PCA.0S.302.CLLC37
7.	Connector		BNC female
8.	Assembly seat	Vertex + Melles Griot	Travel range: 15 mm
9.	Pinhole		Ø: 30 µm
10.	Piezo drive	Physikinstrumente	P-611.XZ0
11.	Pinhole holder		
12.	Piezo holder pt. 2		
13.	Piezo holder pt. 1		
14.	Assembly seat		X,Y,Z travel range: 25 mm

In Figure 7.2, it is shown the minimum and maximum achievable heights, 205 and 240 millimeters respectively, for the objective's axis from the assembly's base. The height adjustment range is 35 millimeters for the objective.

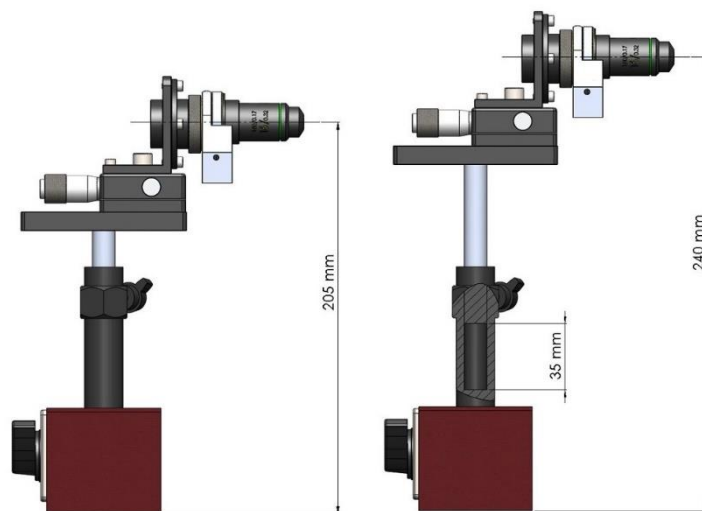


Figure 7.2 - Objective's minimum and maximum height.

To match pinhole height to the objective's height adjustment range two parts were designed, shown below in Figures 7.3-7.5, dimensions are in millimeters:

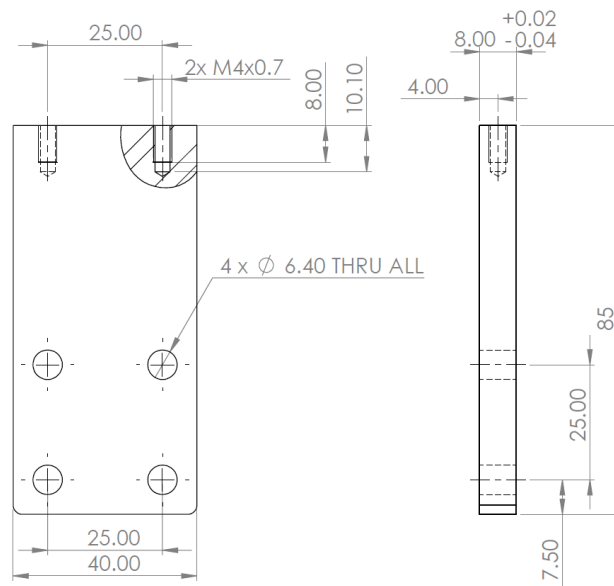


Figure 7.3 - Designed piezo holder part 1

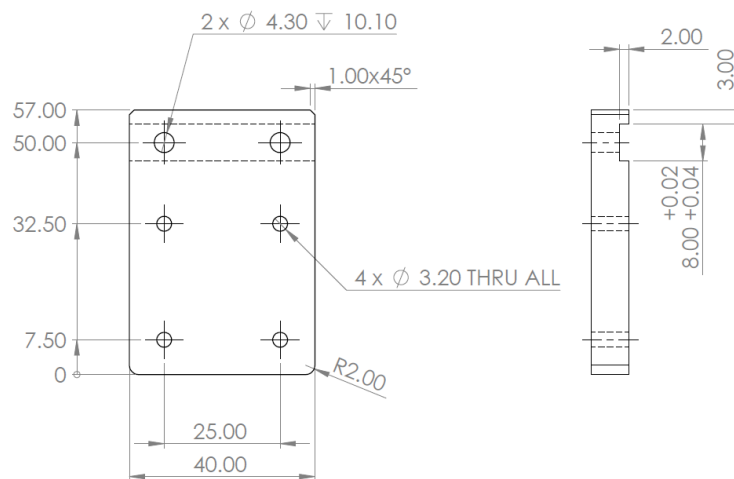


Figure 7.4 - Designed piezo holder part 2

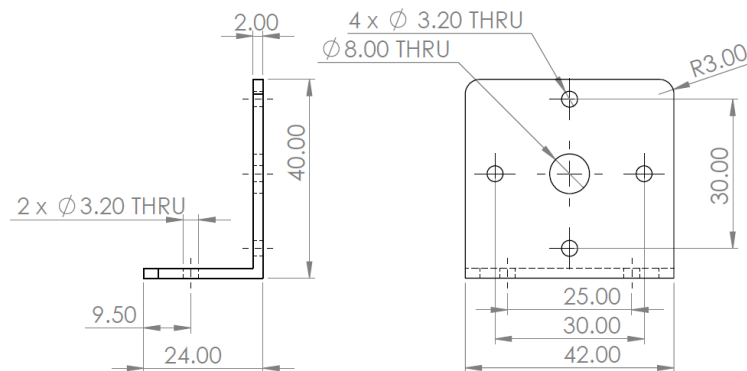


Figure 7.5 - Pinhole holder

The technical drawing of these parts can be found in the Appendix A.

Using these parts for the pinhole assembly we then obtain a minimum and maximum height achievable for the pinhole from its assembly's base of 205 and 230 mm respectively as shown in Figure 7.6.

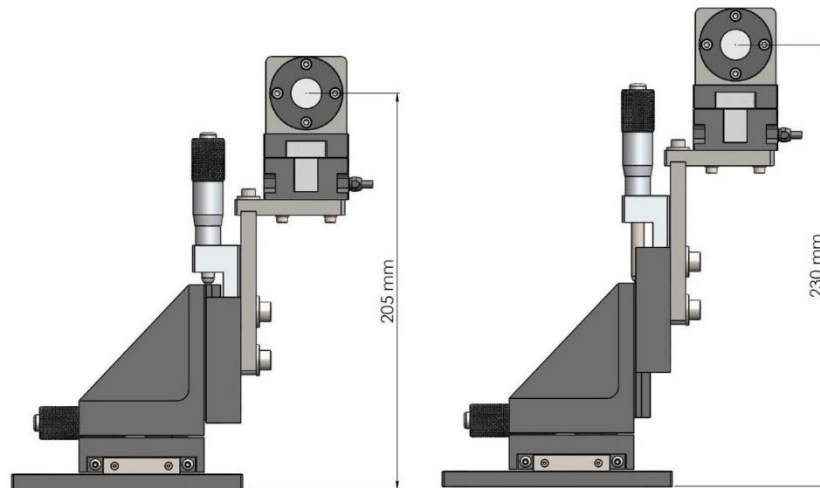


Figure 7.6 - Pinhole's minimum and maximum height.

Taking both assemblies height range into consideration, it is known that the overall height range falls between the 205 and 230 millimeters. Thus, the laser source should also be adjusted at a height between this range.

7.2. Piezo driver - P-611.XZ0

From the company Physikinstrumente, this is a compact two-axis piezo system for nanopositioning [11], with a travel range of $120\ \mu\text{m} \times 120\ \mu\text{m}$ at -20 to $120\ \text{V}$ for open loop, and with resolution of $0.2\ \text{nm}$. This piezo driver is the base for the pinhole, therefore, the pinhole is said to have a travel range of $120 \times 120\ \mu\text{m}$ in the X and Y directions, see Figure 7.7.

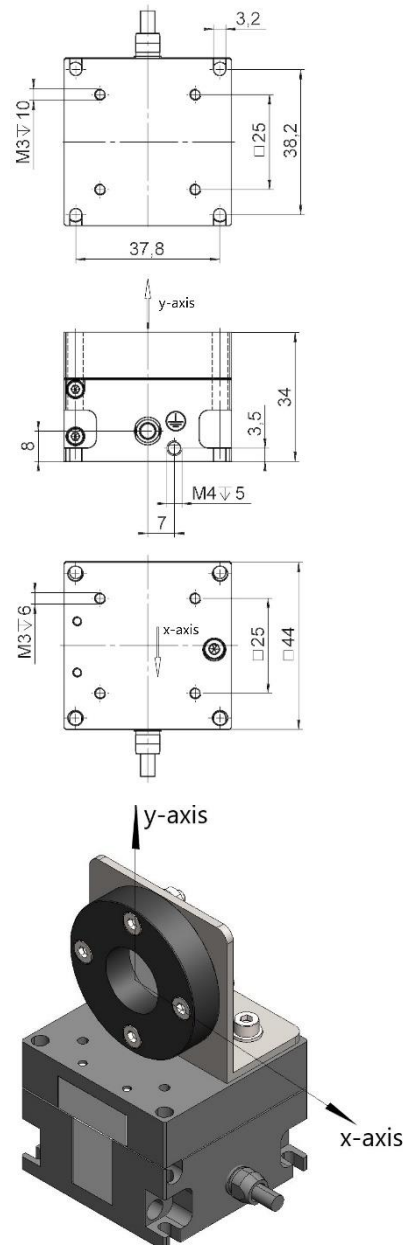


Figure 7.7 - P-611.XZ0 drawing [11] modified, dimensions in mm. And Isometric 3D view with x- and y- axes legend.

7.3. Piezo driver - MIPOS 100

Of the brand Piezosystemjena, this Piezoelectric Objective Positioning System [12] offers a range up to 100 μm in open loop with operational voltage range of -20 to 130 V. Drawing of this driver is shown below:

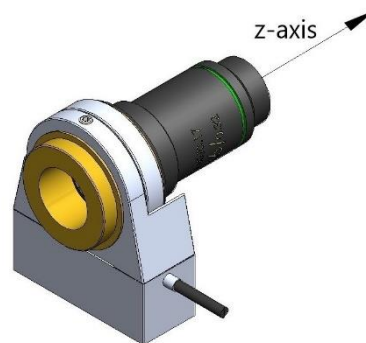
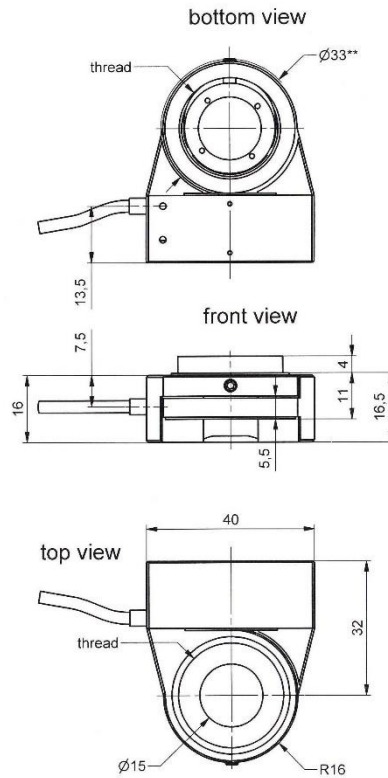


Figure 7.8 - MIPOS 100 drawing [12], dimensions in mm. And isometric 3D view with z- axis legend.

7.4. T-Cube Piezo controller - TPZ001

The T-Cube piezo controller model TPZ001 (discontinued on February 3, 2016) from the company Thorlabs, can be adjusted to a high voltage output range of 75 V, 100 V, or 150 V. As already mentioned, both piezo drivers have an operational voltage range of -20 to 120 V for the P-611.XZ0 and -20 to 130 V in the case of the MIPOS 100. Therefore this controllers are adjusted to an output range of 150 V.



Figure 7.9 - Piezo controller TPZ001 [13].

The graphical user interface (GUI) for this piezo controller can be accessed in MATLAB using the Thorlabs APT ActiveX Control, a single TPZ001 APT GUI is shown below in Figure 7.10.



Figure 7.10 - TPZ001 Piezo Controller Software GUI.

For detailed information on how to implement this or any other Thorlabs APT ActiveX Controller can be found from the downloadable document's link:

https://www.thorlabs.com/images/tabimages/Thorlabs_APT_MATLAB.docx

7.5. Piezo controllers' Hub

As this project would require multi-axis motion (3-axes motions, XYZ), it is then preferred to connect the three controller units to the PC for convenience via USB hub technology. The USB Controller Hub used in this project is the model TCH001 [14], which can support up to six T-Cube controller units.

Table 7.2 - Hub Supply voltage and current requirements.

Supply	Minimum	Maximum	Max Operating Current
+5V	+4.9V	+5.1V	5 A
+15V	+14.5V	+15.5V	6 A
-15V	-14.5V	-15.5V	1 A



Figure 7.11 - T-Cube USB Controller Hub (left), Power Supply Unit (right) [14].

The compact DC power supply unit (PSU) model TPS006 has been designed to power the Controller Hub, and as mentioned in the manual [14], 'the hub must be connected only to this PSU'.

8 GUI Design

The Graphical User Interface designed in the GUIDE Layout Editor of MATLAB for the control and capture of snapshots of the diffraction patterns is shown Figure 8.1, its function is later explained in the Experiment chapter.

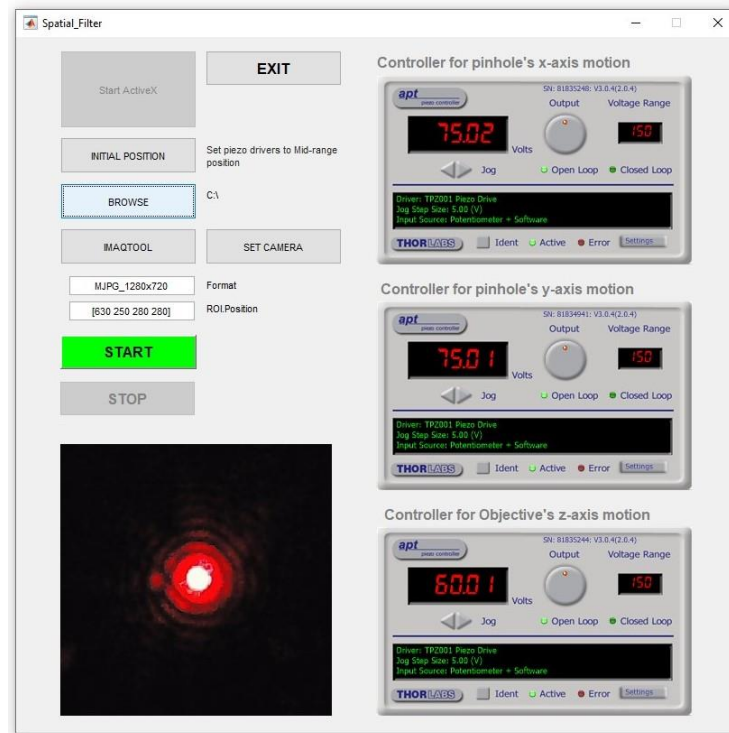


Figure 8.1 - Graphical User Interface for the control and image capture of diffraction patterns.

The images captured by the program are intended to be analyzed to determine the piezo actuator position at which the pattern would show the most circular-shaped diffraction pattern, these images are saved at a grayscale in the selected folder as:

'FigureA_X_Y.jpg'

where:

A = Number of captured image

X = Voltage supplied for the motion in the x-axis direction

Y = Voltage supplied for the motion in the y-axis direction

9 Experiment

The motion in x-, y- and z-axes of the piezo drivers was tested in this experiment with the use of the designed GUI. The setup of this experiment was as shown below in Figure 9.1:

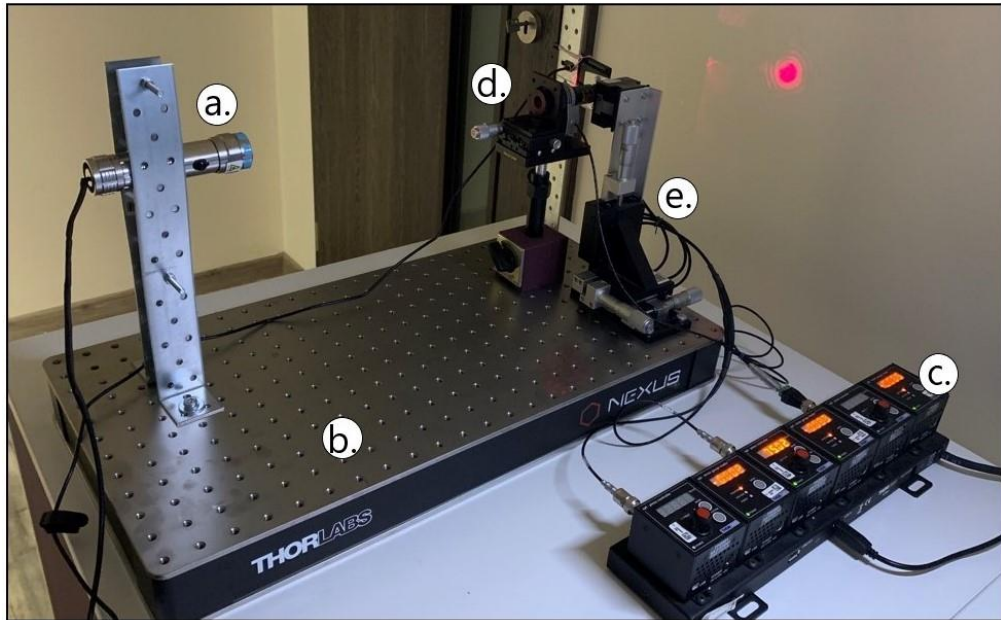


Figure 9.1 - GUI app, piezo driver motion and image capture experimental setup.

The components used in this experiment are as follow:

- a. LUX Tools' Laser pointer source with adapted USB power supply connector [15].
- b. Thorlabs' optical breadboard B3060L [16].
- c. T-Cube USB Controller Hub, with three Piezo controllers TPZ001 and three strain gauge readers (not used), TSG001; connected to its PSU (not shown).
- d. Objective's assembly.
- e. Pinhole's assembly.

9.1. The experiment steps

The experiment was carried as follow:

1. After completion of the equipment setup and adjusting the laser pointer axis to match the objectives axis, then we proceed to run the MATLAB file 'Spatial_Filter.m' which opens the designed GUI shown below in Figure 9.2:

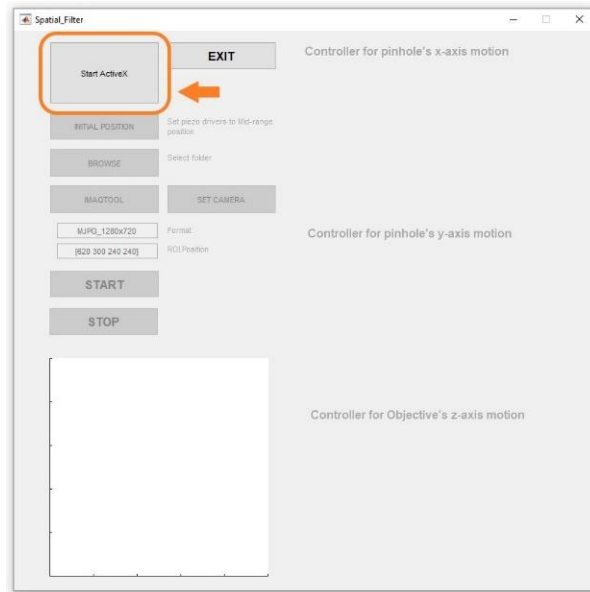


Figure 9.2 - Initiated Spatial Filter application.

2. The button 'Start ActiveX' should then be clicked to make the connection between the application and the TPZ001 Piezo controllers' software GUIs. After the connection has been made the 'INITIAL POSITION' button gets enabled, allowing the user to set both Piezo drivers, P-6110.XZ0 and MIPOS 100, to their mid-range position which was defined from their operational voltage range, them being: 60 V for both axes motions of the P-611.XZ0 and 65 V for the MIPOS 100.

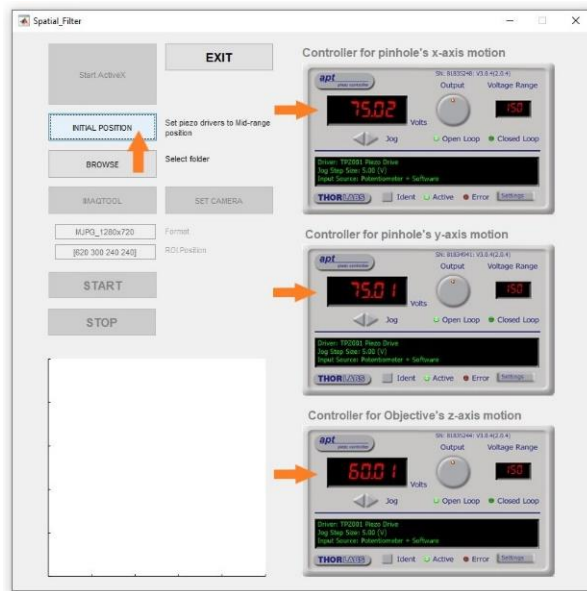


Figure 9.3 - TPZ001 controllers connection initiated.

The mid-range Initial Position has the purpose to let the user adjust the pinhole position manually to a space close enough to where the objective focuses the laser beam and hence, a diffraction pattern can be perceived at the formation plane.

3. The 'BROWSE' button allows the user to select the folder where the snapshot images of the process will be stored.

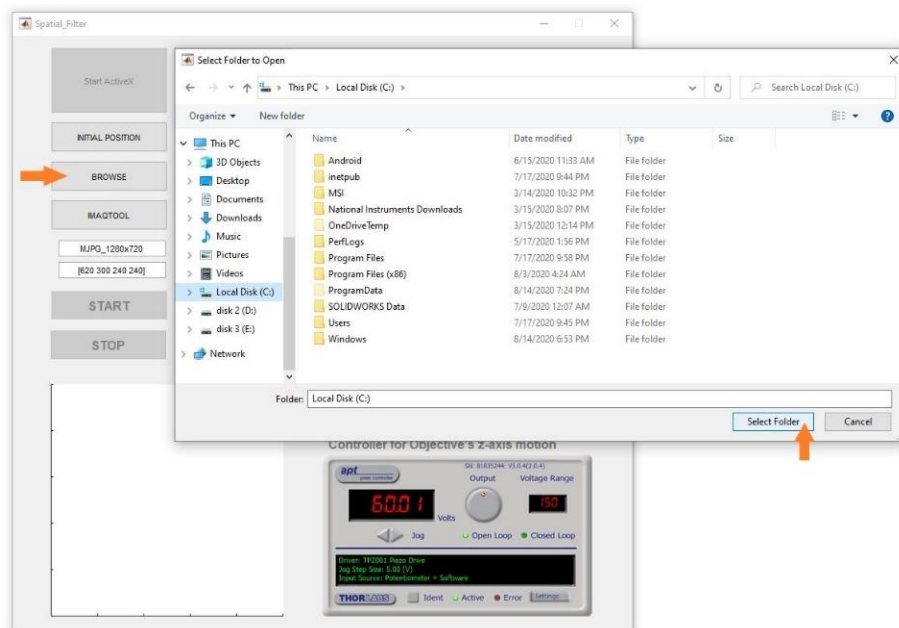


Figure 9.4 - Folder selection for saving images.

As already mentioned, these images are saved in grayscale which is ideal to apply to it the inverse Fast-Fourier Transform in MATLAB. It is recommended to create and store the images in a new folder for easy access in further image analysis.

4. Once completed previous steps and before clicking 'SET CAMERA' button we must first select the Region of Interest from the camera's total view are. Hence, we click the 'IMAQTOOL' button, given this name by the command in MATLAB of `imaqtool` which launches the Image Acquisition Tool. After selection of the camera format (circled in Figure 9.5) will be used and clicking 'Start Preview' the preview for the selected format is shown. In the button tag 'Region of Interest' the button 'Select or Edit' allows to make the selection of only just the region which will be streamed.

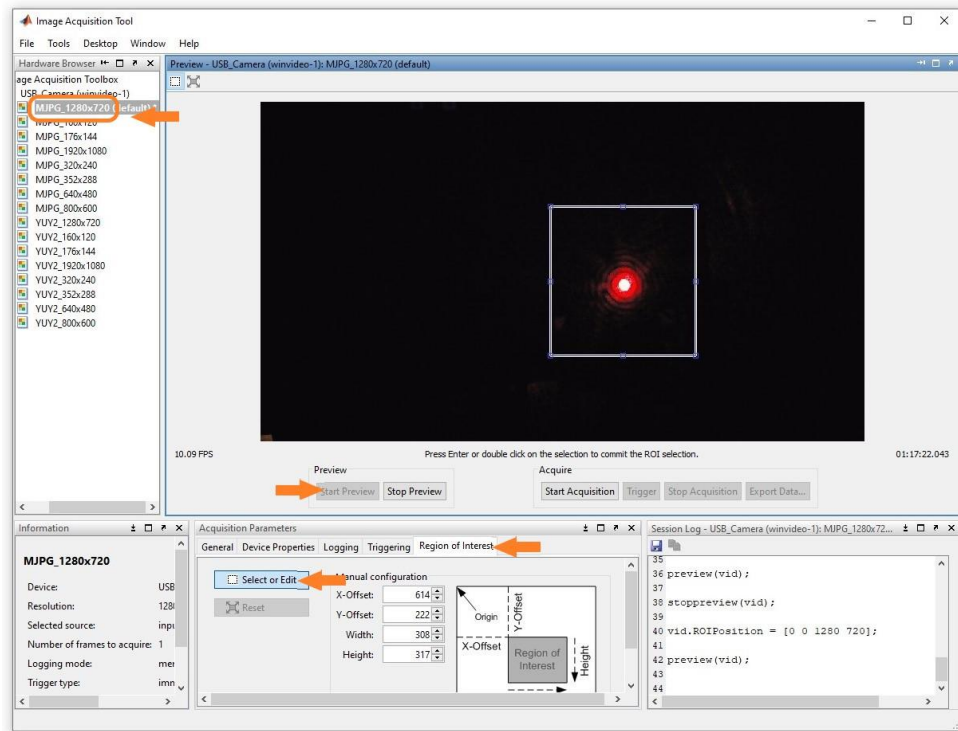


Figure 9.5 - MATLAB's Image Acquisition Tool. Selected camera format and region of interest.

- After Region of Interest (ROI) is defined, click enter. This ROIPosition should be copied (circled), 'Stop preview' and close window.

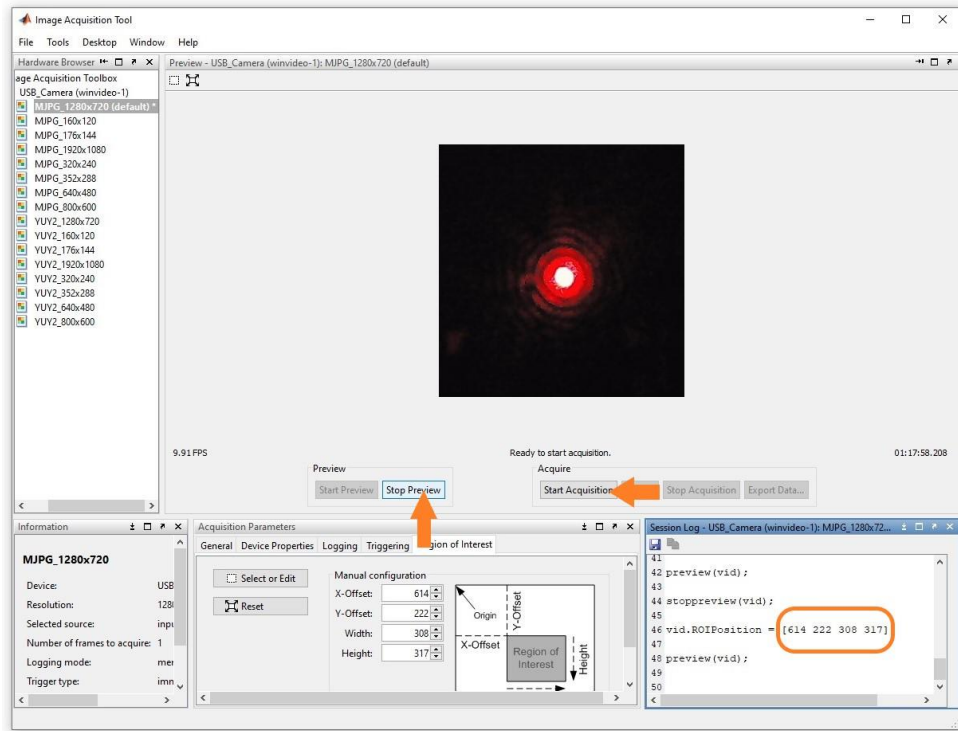


Figure 9.6 - ROIPosition

- Prior pressing 'SET CAMERA', this copied ROI Position must be pasted now into the GUI text box in the application as well as the camera format used to obtain this region of interest. After the user clicks 'SET CAMERA' the video input is then displayed into the application and the XY-axes motion is ready to start.

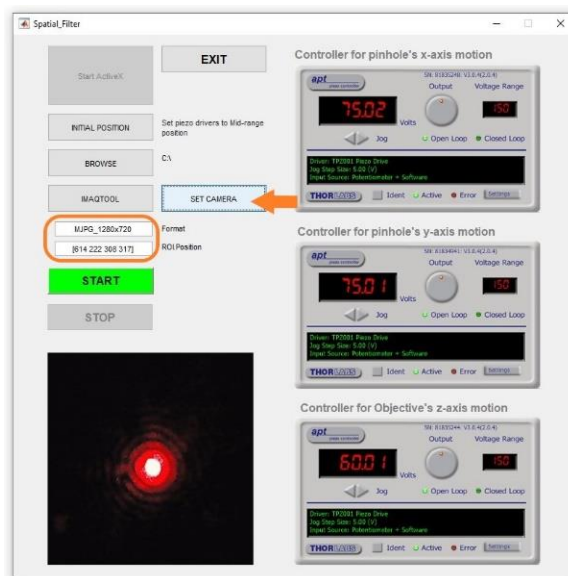


Figure 9.7 - GUI, camera format and ROI position defined.

- Once the process has started, the motion in the X-Y axes takes place, Figure 9.8 shows the obtained diffraction pattern with a supply voltage of 57.66 V, 25 V and 60 V to the piezo drivers for motions X, Y and Z respectively.

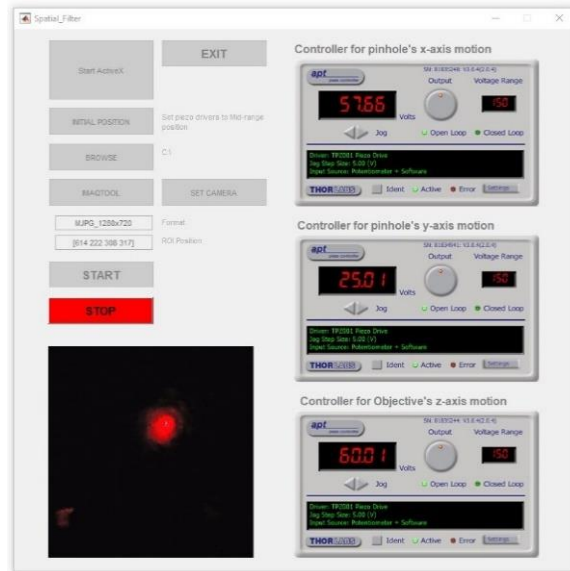


Figure 9.8 - Diffraction pattern shown in the user interface at 57.66V (x-axis), 25V (y-axis) and 60V (z-axis) supply.

9.2. Automatic motion sequence and image capture

Next, it is explained the pinhole's position displacement path for this application.

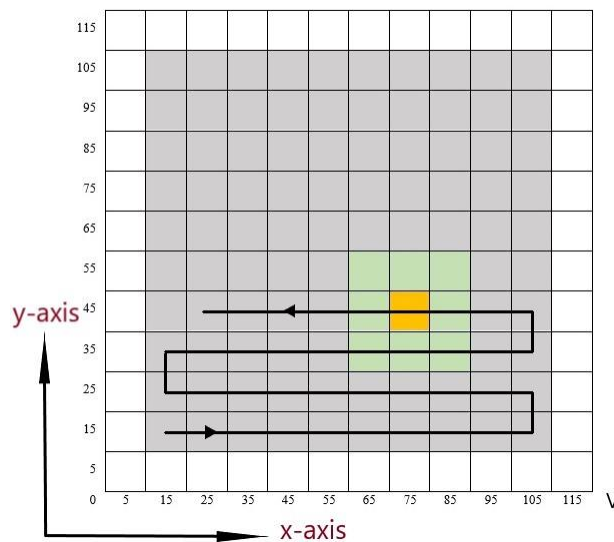


Figure 9.9 - Pinhole's displacement ($1V \approx 1\mu m$).

In Figure 9.9, it is shown the spatial area of the pinhole's displacement for specific input voltage to each one of the motion axis in the piezo driver P-611.XZ0. The 'snake-type' displacement path has step increments of 10 V of input, which may reflect into an approximation of 10 μm displacement. Each of the gray squares represents the area in which a snapshot gets taken, for this case resulting in a total of 100 images, which should then be analyzed to find the nearest-to a perfect Airy-disc pattern (yellow square), thereafter a second iteration could take place to perform the same analysis including surrounding areas (green squares), this area is again divided in same amount of steps, see Figure 9.10. The possible number of iterations which can be done is limited piezo driver P-611-XZ0 which has a displacement resolution of 0.2 nm.

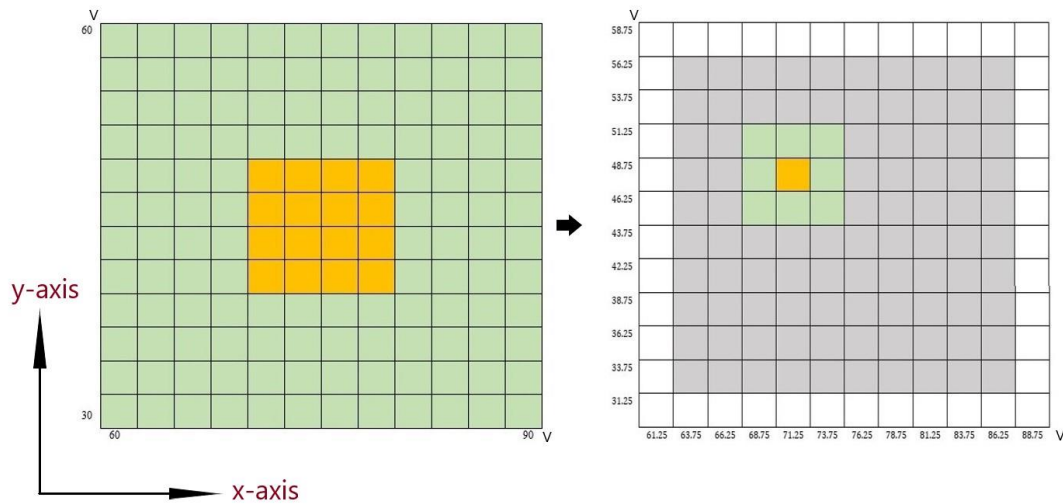


Figure 9.10 - Area of best Airy disk detection (left), becomes next analysis area for the second iteration (right).

This displacement code can be adjusted to have smaller step increments resulting in more images captured in each iteration and therefore reducing the number of iterations needed to obtain same result.

The displacement code:

```
function sequence(handles)
    global xpiezo ypiezo s b v numCapturedImages selpath

    n = 0;
    Iterations = 1;
    rangeV = 120; % input voltage range
    numDiv = 12;
    stepVolt = rangeV/numDiv; % = 10 V
    mid_stepVolt = stepVolt/2; % = 5 V

    numCapturedImages = Iterations*(numDiv-2)^2;
    iteNum=1;

    if s==1
        for ite=1:Iterations
            for y=1:numDiv-2
                Y=y*stepVolt+mid_stepVolt;
                ypiezo.SetVoltOutput(0,Y);
                if n==0
                    for x=1:numDiv-2
                        if b==0
                            break;
                        end
                        X = x*stepVolt+mid_stepVolt;
                        xpiezo.SetVoltOutput(0,X);
                        pause(0.3);
                        img = rgb2gray(getsnapshot(v));
                        imwrite(img, fullfile(selpath, ['figure'
num2str(iteNum) '_' num2str(X) '_' num2str(Y) '.jpg']));

                            iteNum = iteNum + 1;
                            n=1;
                        end
                    elseif n==1
                        for x=1:numDiv-2
                            if b==0
                                break;
                            end
                            X = rangeV-(x*stepVolt+mid_stepVolt);
                            xpiezo.SetVoltOutput(0,X);
                            pause(0.3);
                            img = rgb2gray(getsnapshot(v));
                            imwrite(img, fullfile(selpath, ['figure'
num2str(iteNum) '_' num2str(X) '_' num2str(Y) '.jpg']));

                                iteNum = iteNum + 1;
                                n=0;
                            end
                        end
                    end
                if b==0
                    break;
                end
            end
        end
        iteNum = 1;
    end
end
```

10 Results

The Two-dimensional Fast Fourier Transform was applied in MATLAB to some of the captured images. As seen in the Figure 10.1 below, these 2D Fourier transform images approximately reconstruct the circular shape of the aperture pinhole.

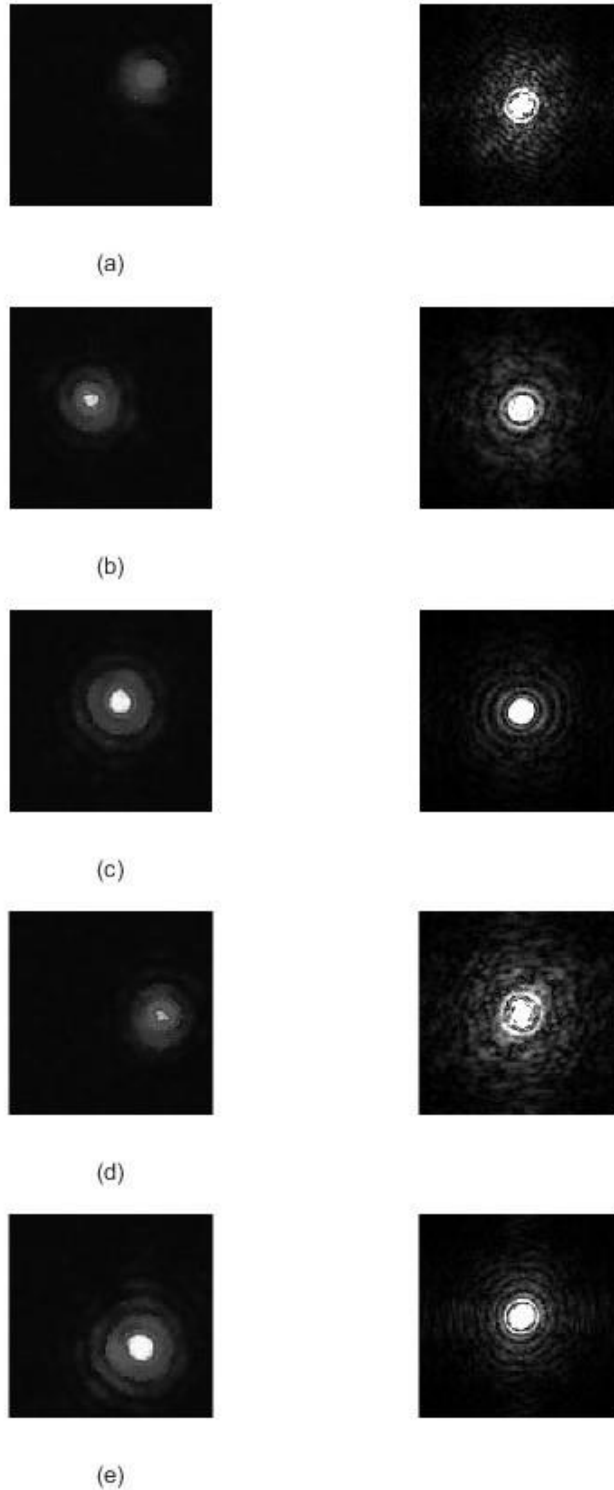


Figure 10.1 - Diffraction patterns (left), and their 2D Fourier Transform (right).

The quality of the 2D Fourier transforms taken of the Diffraction patterns in Figure 10.1 was assessed using the MATLAB functions of `fft2()`, `fftshift()`, `abs()`, `imadjust()` and the Equation (2.2.5) in which the values of M and N are the same of 150 due to the images size of 150x150 pixels.

The used code for obtaining these reconstructed aperture shape images is:

```
clear all; close all; clc;

imgGray = imread('--IMAGE's path name--');

% Reconstruction

imgGrayFFT = (1/150)^2*fft2(imgGray);
imgGrayFFT = fftshift(imgGrayFFT);
imgGrayFFT = abs(imgGrayFFT);
imgGrayFFT = imadjust(imgGrayFFT);

figure(1)
subplot(1,2,1), imshow(imgGray);
subplot(1,2,2), imshow(imgGrayFFT);
```

Those diffraction patterns shown in Figure 10.1 were obtained from the experiment at different pinhole positions from the zero input voltage position point with approximate displacements of:

- (a) 25 μm x 45 μm .
- (b) 95 μm x 65 μm .
- (c) 55 μm x 65 μm .
- (d) 15 μm x 75 μm .
- (e) 35 μm x 105 μm .

The Region point at which each of these analyzed images was taken can be seen in the X-Y axes map below in Figure 10.2:

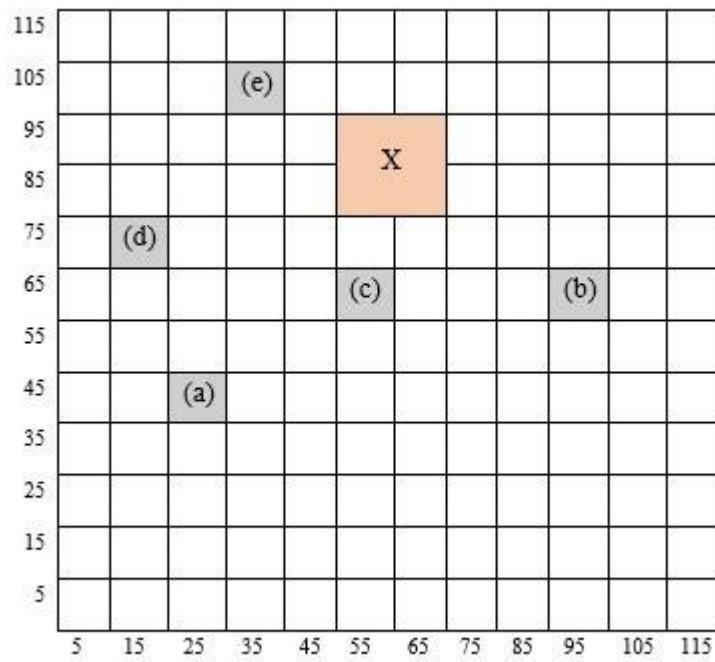


Figure 10.2 - Region of analysed images.

It can be deduced by intuition that the region where the Airy disk's diffraction patterns would result in a more symmetric shape is within (or near) the X-marked area.

A proposed way of analysing symmetry in the Airy disc would be by plotting the Cross-sections in the X and Y axes of the image's intensity at the center point of the highest intensity point in the image as shown in Figure 10.3.

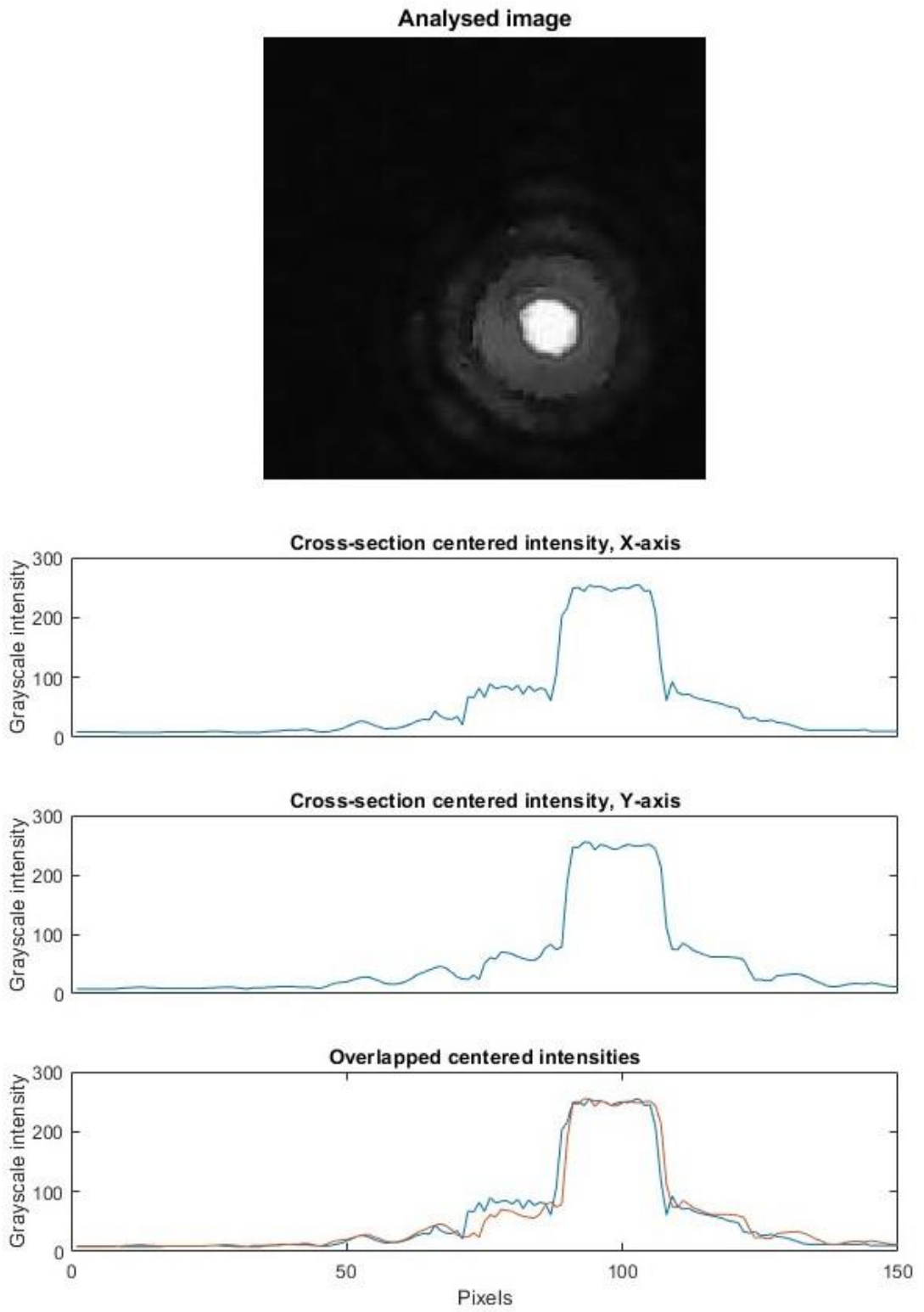


Figure 10.3 - Proposed Symmetry analysis for next development.

11 Conclusion

After getting acquainted with the basic theory in Fourier Optics & the Diffraction phenomena as well as getting familiarized with the functionality of Spatial Filter it was clear it would be best to create this work with the use of software MATLAB, which provides rather simple ways of handling images to further develop a better analysis.

In sum, all goals initially set have been fulfilled. The method used during image processing (diffraction reconstruction, as seen in Figure 10.1) is very straightforward because the equations described in this thesis are rather explanatory as the MATLAB software performs all the computation needed with a simple call of these function.

There is plenty of more work and analysis which should be done for future development of the automatic adjustment for full functionality just like the proposed Symmetry analysis. With MATLAB's image processing tools more methods could be proposed.

Appendix A

Contents of the attached CD

- **Spatial_Filter.m** – main code.
- **Spatial_Filter.fig** – GUI's configurable figure file.
- **sequence.m** – the pinhole's displacement code.
- **Piezo holder part 1.pdf** – designed part pdf drawing file.
- **Piezo holder part 2.pdf** – designed part pdf drawing file.
- **Pinhole holder.pdf** – designed part pdf drawing file.
- **FraunhoferDiffraction.mlapp** – Fraunhofer's Diffraction simulation.

Bibliography

- [1] J. Heikenfeld. [Online]. Available: <http://noveldevicelab.com/files/2018-11/Week 6 - Fourier Optics.pdf>. [Accessed 02 07 2020].
- [2] B. Huang. [Online]. Available: <https://www.ibiology.org/talks/fourier-transform/>. [Accessed 10 07 2020].
- [3] Wikipedia, "Joseph Fourier," [Online]. Available: https://es.wikipedia.org/wiki/Joseph_Fourier. [Accessed 02 07 2020].
- [4] T.-C. Poon and P. P. Banerjee, in *Contemporary optical image processing with MATLAB*, Oxford, ELSEVIER SCIENCE Ltd, 1996, p. 33.
- [5] R. C. Gonzalez ja R. E. Woods, *Digital Image Processing*, Upper Saddle River, NJ: Prentice-Hall, 2001.
- [6] "MathWorks Help Center," [Online]. Available: <https://www.mathworks.com/help/matlab/ref/fft.html>. [Accessed 16 07 2020].
- [7] H. University. [Online]. Available: <http://optics.hanyang.ac.kr/~shsong/P4-Fourier%20optics.pdf>. [Accessed 04 07 2020].
- [8] Wikipedia, "Diffraction," [Online]. Available: <https://en.wikipedia.org/wiki/Diffraction>. [Accessed 20 07 2020].
- [9] HyperPhysics, "Circular Aperture Diffraction," [Online]. Available: <http://hyperphysics.phy-astr.gsu.edu/hbase/phyopt/cirapp2.html#c2>. [Accessed 22 07 2020].
- [10] Thorlabs, "Principles of Spatial Filters," [Online]. Available: https://www.thorlabs.com/newgrouppage9.cfm?objectgroup_id=10768. [Accessed 15 04 2020].
- [11] "PI motion positioning," Physikinstrumente, [Online]. Available: <https://www.physikinstrumente.com/en/products/nanopositioning-piezo-flexure-stages/xy-piezo-flexure-stages/p-611xz-p-6112-xz-xy-nanopositioner-201725/>. [Accessed 28 07 2020].
- [12] Piezosystemjena, [Online]. Available: https://www.piezsystem.com/products/piezo_actuators/mipos/mipos_100/. [Accessed 28 07 2020].

- [13] Thorlabs, [Online]. Available:
<https://www.thorlabs.com/drawings/3120d9bed59837ef-C029D767-C403-DD1A-08E932A28CFABB7A/TPZ001-APTManual.pdf>. [Accessed 28 07 2020].
- [14] "TCH001 Manual," [Online]. Available:
<https://www.thorlabs.com/drawings/3120d9bed59837ef-C029D767-C403-DD1A-08E932A28CFABB7A/TCH001-Manual.pdf>. [Accessed 29 07 2020].
- [15] LUX tools, [Online]. Available: <https://www.obi.cz/kapesni-svitilny/lux-sada-kapesnich-svitilen-led-2dilna-vcetne-funkce-laseru/p/4687448>. [Accessed 05 08 2020].
- [16] Thorlabs, [Online]. Available:
<https://www.thorlabs.de/thorproduct.cfm?partnumber=B3060L>. [Accessed 07 08 2020].